https://dx.doi.org/10.1016/j.compstruct.2019.111813

Vibrations of Graphene Nanoplatelet Reinforced Functionally Gradient Piezoelectric Composite Microplate Based on Nonlocal Theory

J. J. Mao[a1], H. M. Lu[a2], W. Zhang[a3*] and S. K. Lai[b4]

[a]Beijing Key Laboratory of Nonlinear Vibrations and Strength of Mechanical Structures
College of Mechanical Engineering, Beijing University of Technology
Beijing 100124, P. R. China

[b]Department of Civil and Environmental Engineering, The Hong Kong Polytechnic University, Hong Kong, P. R. China

[1]Email: jiajia.mao@bjut.edu.cn, [2]Email: luhaoming@emails.bjut.edu.cn
[3]Email: sandyzhang0@yahoo.com, [4]Email: sk.lai@polyu.edu.hk

Running Headline: Vibrations of Graphene Nanoplatelet Reinforced Microplate

* corresponding author, email: sandyzhang0@yahoo.com

Abstract

This paper investigates the small-scale effect on the linear and nonlinear vibrations of the graphene nanoplatelet (GNPL) reinforced functionally gradient piezoelectric composite microplate based on the nonlocal constitutive relation and von Karman geometric nonlinearity. The GNPL reinforced functionally gradient piezoelectric composite microplate is resting on the Winkler elastic foundation and is subjected to an external electric potential. The parallel model of Halpin Tsai is used to compute the effective Young's modulus of the GNPL reinforced functionally gradient piezoelectric composite microplate. The Poisson's ratio, mass density and piezoelectric properties of the GNPL reinforced functionally gradient piezoelectric composite microplate are calculated by using the rule of mixture. Hamilton's principle is adopted to obtain the higher-order nonlinear partial differential governing equations of motion for the GNPL reinforced functionally gradient piezoelectric composite microplate. The partial differential governing equations of motion are reduced to a system of the nonlinear algebraic eigenvalue equations by using the differential quadrature (DQ) method and are solved by an iteration progress. The efficiency and accuracy of the present approach are verified by comparing with the existed results. Both uniformly and functionally distributing graphene nanoplatelets (GNPLs) are considered to investigate the effects of the GNPL concentration, external voltage, nonlocal parameter, geometrical and piezoelectric characteristics of the GNPLs as well as the elasticity coefficient of the Winkler elastic foundation on the linear and nonlinear dynamic behaviors of the GNPL reinforced functionally gradient piezoelectric composite microplate with various boundary conditions. The numerical results clearly manifest that the GNPLs can significantly enhance the structural stiffness of the micro-electro-mechanical system (MEMS).

Keywords: Linear and nonlinear vibrations; GNPL reinforced functionally gradient piezoelectric composite microplate; nonlocal theory; small-scale effect

1. Introduction

The graphene nanoplatelets (GNPLs) have attracted considerable industrial and academic attentions because of their excellent mechanical, thermal and electrical properties [1-3]. The Young's modulus of the epoxy nanocomposites with 0.1% weight fraction of the graphene nanoplatelet (GNPL) reinforcements is increased to 131% compared with the pure epoxy [4]. The storage modulus, stress at the break and Young's modulus of the PVDF matrix are respectively increased to 124%, 97% and 121% by adding 0.75% volume fraction of the GNPLs [5]. With the addition of graphite, the electrical conductivity of the epoxy nanocomposites obtained an increase of 12 times [6].

In the last two decades, functionally graded materials (FGMs) are very popular for enhancing the static and dynamic characteristics of the structures [7,8] even in the environment with the high temperature due to their continuous and smooth manner [9]. Zhang and his co-authors organized a serial valuable work to explore the nonlinear dynamic behaviors of the functionally graded material (FGM) structures, including the FGM plate [8,10-13] and FGM shell [14] under different operating conditions. Recently, Yang's group [15] introduced the GNPL reinforced functionally gradient multilayer composites, in which the GNPLs meet a layer mode along the thickness direction and also made a series of valuable research about the static and dynamic behaviors of the GNPL reinforced functionally gradient beams and plates using the classical continuum theories [15-17]. Their results illustrated that a small amount of GNPLs spreading in the polymer matrix can significantly enhance the static and dynamic responses of the GNPL reinforced functionally gradient beams and plates. Shen and his co-authors [18-20] took into account the interaction of the varying temperature and foundation excitation to investigate the linear and nonlinear behaviors of the GNPL reinforced functionally gradient structures through the third-order shear deformation theory. Kiani [21] investigated the large amplitude free vibration of the graphene sheet reinforced laminated plates based on the finite elements, the third-order shear deformation theory and non-uniform reasonable B-spline shape functions.

The piezoelectric materials have been widely used in the smart structures and electromechanical systems [22,23] because of their excellent electro-mechanical coupling behaviors. Song et al. [24] achieved the active control of carbon nanotube strengthen composite cylindrical shells using the piezoelectric patches. Zhang et al. [25] investigated the 1:2 internal resonance of the composite laminated piezoelectric rectangular plate. Zhang and Hao [26] studied the global bifurcations and multi-pulse chaotic dynamics of a composite laminated piezoelectric rectangular plate with four-edge simply supported. Zhang and his coauthors analyzed the chaotic dynamic behaviors of the laminated composite piezoelectric rectangular plate [27] and beam [28]. Selim et al. [29] proposed the position of the piezoelectric sensor to control the vibrations of the carbon nanotube reinforced composite plate. Zhang et al. [30] conducted the active flutter control of the cylindrical nanocomposite under the supersonic airflow and the thermal environments. Zhang et al. [31] found that the dynamic characteristics of the piezoelectric plate are particularly sensitive to the forcing and parametric excitations. Lu et al. [32] investigated the nonlinear vibrations of the deploying cantilevered composite laminated plate under combined the aerodynamic load and piezoelectric excitation.

Many opening literatures demonstrated that the GNPL reinforcements can strengthen the dielectric, mechanical, piezoelectric, pyroelectricity properties and structural stiffness of the piezoelectric composite structures [5,33-34]. Mao et al. studied the linear and nonlinear vibrations [35] and the buckling and postbuckling behaviors [36] of the GNPL reinforced PVDF composite macroplates. They indicated that the GNPL nanofillers can significantly improve the static and dynamic behaviors of the PVDF composite microplates. Guo et al. [37] considered von Karman geometric nonlinear relationship of the composite laminated plates with the graphene skin to analyze their dynamic behaviors. Xu et al.'s experiments [38] found that the suspended graphene layers have the positive piezoconductive effect. This effect is closely relevant to the number of graphene layers. Abolhasani et al. [39] prepared the graphene reinforced polyvinylidene fluoride (PVDF) composite nanofibers successfully and firstly investigated their polymorphism, morphology, crystallinity and electrical outputs experimentally. According to the present research, there is a great potential value for the GNPLs using in the fields of flexible electronics and sensing technology [40], especially for the micro- and nano- electromechanical systems (MEMS and NEMS).

For the micro- and nano- structures, the experimental studies observed the small size effects on the mechanical properties [41-43]. The classical elasticity theory is unable to explain the size effects since it does not involve a material length scale. To model and analyze the small-sized mechanical structures, many size-dependent theories which can capture the size effects were proposed and developed [44-48]. One of the well-known models is the nonlocal elasticity theory [48], which includes both the scale effects and the long-range atomic interactions. Reddy [49] developed the nonlocal theory to analyze the nonlinear bending of the isotropic nanoplates with the classical and shear deformations based on von Karman nonlinearity. Ke and his group [50,51] discussed the linear and nonlinear vibrations of the piezoelectric nanoplates with various boundary conditions under the effects of the multi-field coupling, including the thermo-electro-mechanical and electro-mechanical through the nonlocal theory. With the governing equations of the nonlocal plate model, Zhang et al. [52-54] employed the element-free KP-Ritz method to solve the natural frequencies [52], nonlinear deflections [53] and buckling loads [54] of the single-layered graphene nanosheets.

The references involving the small size effects of the graphene reinforced composite structures are very limited. Only Sahmani and his colleagues [55,56] considered the nonlocal size effects to investigate the nonlinear bending and instability behaviors of the GNPL reinforced functionally graded porous micro- and nano-beams [55] and shells [56]. Moreover, there is no public report to research the static and dynamic behaviors of the GNPL reinforced piezoelectric composite structures by considering the influence of the small size.

This paper investigates the small-scale effect on the linear and nonlinear vibrations of the GNPL reinforced functionally graded piezoelectric composite microplate, which is resting on the Winkler elastic foundation and subjected to an external electric potential, based on the nonlocal constitutive relation and von-Karman geometric nonlinearity. The GNPLs are assumed to be respectively uniformly and graded distributing in the PVDF matrix. The parallel model of Halpin Tsai is introduced to compute the effective Young's modulus of the GNPL reinforced functionally graded piezoelectric composite microplate. The Poisson's ratio, mass density and piezoelectric properties of the GNPL reinforced functionally graded piezoelectric composite microplate are deduced by using the rule of mixture. The higher-order nonlinear partial differential governing equation of motion for the GNPL reinforced functionally graded piezoelectric composite microplate is established by Hamilton's principle. The differential quadrature (DQ) method and the iteration progress are utilized to solve the nonlinear partial differential governing equation of motion for the GNPL reinforced functionally graded piezoelectric composite microplate. The effects of the external voltage, nonlocal parameter, GNPL distributing pattern and concentration, geometric and piezoelectric characteristics of GNPLs, elasticity coefficient of the Winkler elastic foundation as well as the boundary conditions on the linear and nonlinear vibration characteristics are studied for the nonlocal GNPL reinforced functionally graded piezoelectric composite microplate in detail.

2. Theoretical Formulation

Figure 1 demonstrates a GNPL reinforced functionally graded piezoelectric composite microplate which is subjected to an external electric potential $\hat{\phi}$ and is rested on the Winkler elastic foundation in the Cartesian coordinate system. The length, width and thickness of the GNPL reinforced functionally graded piezoelectric composite microplate respectively are a, b and h. The GNPL reinforced functionally graded piezoelectric composite microplate consists of N GNPL reinforced piezoelectric layers with equal thickness $\Delta h = h_M / N$, where N is an even number. Both the uniform and the graded distributing forms of the GNPLs are explored, as shown in Figure 2. In each GNPL reinforced piezoelectric layer, the GNPLs distribute uniformly. For the U pattern, the concentration of the GNPL reinforced piezoelectric layer keeps same along the thickness of the GNPL reinforced piezoelectric composite microplate. However, for the X and O patterns, the concentration respectively increases and decreases symmetrically and linearly from the middle layer to the top and bottom layers. In Figure 2, the varying concentration is expressed by the different colors of the GNPL reinforced piezoelectric layers, in which the darker color represents the bigger GNPL volume fraction. As seen in Figure 2, the top and bottom layers of the X pattern are darker than the middle layers, which means that either sides have more GNPL reinforcements than the middle layers. Inversely, the middle layers have the darker color for the O pattern microplate.

Assuming the integral volume fractions V_{gpl}, NV^* and V^* of the GNPLs for the GNPL reinforced functionally graded piezoelectric composite microplate are respectively the maximum and minimum volume fractions in the X and O patterns. We have the following equation

$$V^* = \frac{2}{1+\frac{N}{2}} \cdot V_{gpl} \,. \tag{1}$$

Since the content of the GNPLs in the X and O patterns varies linearly layer by layer, the volume fractions of the GNPLs in the k-th layer of the GNPL reinforced functionally graded piezoelectric composite microplate are expressed as

for the X pattern

$$V_k = \left(\frac{N}{2} + 1 - k\right) V^* \text{, when } k \le \frac{N}{2} \,, \tag{2a}$$

$$V_k = \left(k - \frac{N}{2}\right) V^*, \text{ when } k \geq \frac{N}{2}, \tag{2b}$$

and for the O pattern

$$V_n = k\, V^*, \text{ when } k \leq \frac{N}{2}, \tag{3a}$$

$$V_k = \left(N + 1 - k\right) V^*, \text{ when } k \geq \frac{N}{2}. \tag{3b}$$

Moreover, the GNPL volume fraction of the *k*-th GNPL reinforced piezoelectric layer is equal to V_{gpl} for the U pattern.

The GNPLs are easier to disperse into the composite when the content of the GNPLs is less than 1% [57]. In addition, the experimental results given by Layek et al. [5] manifested that the GNPL reinforcements tend to parallelly disperse into the PVDF matrix when the GNPL content is not higher than 1%. The parallel model of Halpin Tsai is valid when we calculate the Young's modulus of the novel material [5]. The PVDF composite microplate considered in the present paper is reinforced by the perfectly bonded rectangular GNPLs with the length a_{gpl}, width b_{gpl} and thickness h_{gpl}. Besides, we have $V_{gpl} \leq 1\%$. The Young's modulus E_n of the *k*-th GNPL reinforced piezoelectric layer is expressed as

$$E_k = \frac{1 + \dfrac{2a_{gpl}}{3h_{gpl}} \eta_L V_n}{1 - \eta_L V_n} E_M, \tag{4}$$

where

$$\eta_L = \frac{\dfrac{E_G}{E_M} - 1}{\dfrac{E_G}{E_M} + \dfrac{2a_{gpl}}{3h_{gpl}}}, \tag{5}$$

and the subscripts "*M*" and "*G*" respectively indicate the PVDF matrix and GNPLs.

The Poisson's ratio ν, mass density ρ, piezoelectric constant e_{im} and dielectric constant κ_{im} of the *k*-th GNPL reinforced piezoelectric layer are calculated by the mixed law

$$\nu_k = \nu_G V_k + \nu_M (1 - V_k), \tag{6a}$$

$$\rho_k = \rho_G V_k + \rho_M (1 - V_k), \tag{6b}$$

$$e_{im,k} = e_{im,G} V_k + e_{im,M} (1 - V_k), \tag{6c}$$

$$\kappa_{im,k} = \kappa_{im,G} V_k + \kappa_{im,M} (1 - V_k). \tag{6d}$$

According to the first-order shear deformation plate theory (FSDT), the displacement field $u_1(x,y,z,t)$, $u_2(x,y,z,t)$ and $u_3(x,y,z,t)$ of an arbitrary point along the *x*, *y* and *z* directions are respectively expressed as

$$u_1(x,y,z,t)=U(x,y,t)+z\varphi_x(x,y,t), \tag{7a}$$

$$u_2(x,y,z,t)=V(x,y,t)+z\varphi_y(x,y,t), \tag{7b}$$

$$u_3(x,y,z,t)=W(x,y,t), \tag{7c}$$

where $U(x,y,t)$, $V(x,y,t)$ and $W(x,y,t)$ are the displacement components on the mid-plane of the GNPL reinforced functionally graded piezoelectric composite microplate, $\varphi_x(x,y,t)$ and $\varphi_y(x,y,t)$ are respectively the cross section rotations about the y and x axes, and t is time.

Based on von-Karman large deformation theory, the relationship between the strain and displacement is written as

$$\begin{Bmatrix} \varepsilon_{xx} \\ \varepsilon_{yy} \\ 2\varepsilon_{xz} \\ 2\varepsilon_{yz} \\ 2\varepsilon_{xy} \end{Bmatrix} = \begin{Bmatrix} \varepsilon_{xx}^{(0)} \\ \varepsilon_{yy}^{(0)} \\ 2\varepsilon_{xz}^{(0)} \\ 2\varepsilon_{yz}^{(0)} \\ 2\varepsilon_{xy}^{(0)} \end{Bmatrix} + z\begin{Bmatrix} \varepsilon_{xx}^{(1)} \\ \varepsilon_{yy}^{(1)} \\ 2\varepsilon_{xz}^{(1)} \\ 2\varepsilon_{yz}^{(1)} \\ 2\varepsilon_{xy}^{(1)} \end{Bmatrix}, \tag{8}$$

where ε_{xx} and ε_{yy} are respectively the normal strains along the *x* and *y* axes, $2\varepsilon_{xy}$, $2\varepsilon_{yz}$ and $2\varepsilon_{xz}$ are separately the shear strains along the *x*O*y*, *y*O*z* and *x*O*z* planes, and we have

$$\begin{Bmatrix} \varepsilon_{xx}^{(0)} \\ \varepsilon_{yy}^{(0)} \\ 2\varepsilon_{xz}^{(0)} \\ 2\varepsilon_{yz}^{(0)} \\ 2\varepsilon_{xy}^{(0)} \end{Bmatrix} = \begin{Bmatrix} \dfrac{\partial U}{\partial x}+\dfrac{1}{2}\left(\dfrac{\partial W}{\partial x}\right)^2 \\ \dfrac{\partial V}{\partial y}+\dfrac{1}{2}\left(\dfrac{\partial W}{\partial y}\right)^2 \\ \dfrac{\partial W}{\partial x}+\varphi_x \\ \dfrac{\partial W}{\partial y}+\varphi_y \\ \dfrac{\partial U}{\partial y}+\dfrac{\partial V}{\partial x}+\dfrac{\partial W}{\partial x}\dfrac{\partial W}{\partial y} \end{Bmatrix}, \tag{9a}$$

and

$$\begin{Bmatrix} \varepsilon_{xx}^{(1)} \\ \varepsilon_{yy}^{(1)} \\ 2\varepsilon_{xz}^{(1)} \\ 2\varepsilon_{yz}^{(1)} \\ 2\varepsilon_{xy}^{(1)} \end{Bmatrix} = \begin{Bmatrix} \dfrac{\partial \varphi_x}{\partial x} \\ \dfrac{\partial \varphi_y}{\partial y} \\ 0 \\ 0 \\ \dfrac{\partial \varphi_x}{\partial y} + \dfrac{\partial \varphi_y}{\partial x} \end{Bmatrix}. \tag{9b}$$

To investigate the linear and nonlinear vibrations of the GNPL reinforced functionally graded piezoelectric composite microplate, the extended Eringen's nonlocal elasticity theory [48] is employed. The stress at a certain point x in the body not only depends on the strain of this tiny point, but also relies on the electric field and stress field of other points x' around the reference point x.

The nonlocal integral constitutive relations of a homogeneous and isotropic piezoelectric solid can be written as [50,51]

$$\sigma_{ij} = \int_{\Lambda} \alpha(|x' - x|, \tau) \left[Q_{ijnl} \varepsilon_{nl}(x') - e_{nij} E_n^{(\phi)}(x') \right] dx', \tag{10a}$$

$$D_i = \int_{\Lambda} \alpha(|x' - x|, \tau) \left[e_{inl} \varepsilon_{nl}(x') - \kappa_{nij} E_n^{(\phi)}(x') \right] dx', \tag{10b}$$

where Λ represents the volume of the piezoelectric solid, σ_{ij} is the stress component, ε_{ij} indicates the strain component, D_i and $E_i^{(\phi)}$ respectively represent the components of the electrical displacement and electric field, Q_{ijnl}, e_{nij} and κ_{nij} respectively denote the elastic constant, piezoelectric constant and dielectric constant, $\alpha(|x' - x|, \tau)$ is the nonlocal attenuation function, in which $|x' - x|$ is the Euclidean distance, $\tau = e_0 a_0 / l$ is the scale modulus which merges the small scale factor, e_0, a_0 and l are separately the material coefficient which is always obtained experimentally, internal and external natural lengths of the nanostructures.

Ignoring the body force density, the nonlocal integral constitutive relations are rewritten as equivalent differential form [50,51]

$$\sigma_{ij,j} = \rho \ddot{u}_i, \tag{11a}$$

$$D_{i,i} = 0, \tag{11b}$$

$$E_i = -\hat{\phi}_{,i}, \tag{11c}$$

where equations (11a)-(11c) are respectively the kinematic equation, Maxwell equation and relation between electric potential and electric field, u_i and ρ are respectively the components of the displacement and mass density.

Under the assumption on each GNPL reinforced piezoelectric layer is homogeneous and isotropic, the nonlocal constitutive relations of the k-th GNPL reinforced piezoelectric layer are rewritten as

$$\sigma_{ij} - (e_0 a_0)^2 \nabla^2 \sigma_{ij} = Q_{ijnl} \varepsilon_{nl} - e_{ijn} E_n^{(\phi)}, \tag{12a}$$

$$D_i - (e_0 a_0)^2 \nabla^2 D_i = e_{inl} \varepsilon_{nl} - \kappa_{nij} E_n^{(\phi)}, \tag{12b}$$

where $e_0 a_0$ is the scale coefficient revealing the size effect on the response of the structures in the nano- and micro-sizes, and ∇^2 is the Laplace operator.

Therefore, the constitutive equations of the k-th GNPL reinforced nonlocal piezoelectric layer for the GNPL reinforced functionally graded piezoelectric composite microplate are approximated as

$$\begin{Bmatrix} \sigma_{xx} \\ \sigma_{yy} \\ \sigma_{xz} \\ \sigma_{yz} \\ \sigma_{xy} \end{Bmatrix}_{(k)} - (e_0 a)^2 \nabla^2 \begin{Bmatrix} \sigma_{xx} \\ \sigma_{yy} \\ \sigma_{xz} \\ \sigma_{yz} \\ \sigma_{xy} \end{Bmatrix}_{(k)} = \begin{Bmatrix} Q_{11} & Q_{12} & 0 & 0 & 0 \\ Q_{12} & Q_{22} & 0 & 0 & 0 \\ 0 & 0 & Q_{55} & 0 & 0 \\ 0 & 0 & 0 & Q_{44} & 0 \\ 0 & 0 & 0 & 0 & Q_{66} \end{Bmatrix}_{(k)} \begin{Bmatrix} \varepsilon_{xx} \\ \varepsilon_{yy} \\ 2\varepsilon_{xz} \\ 2\varepsilon_{yz} \\ 2\varepsilon_{xy} \end{Bmatrix}_{(k)}$$

$$- \begin{bmatrix} 0 & 0 & e_{31} \\ 0 & 0 & e_{32} \\ 0 & 0 & 0 \\ 0 & e_{24} & 0 \\ e_{15} & 0 & 0 \end{bmatrix}_{(k)} \begin{Bmatrix} E_x \\ E_y \\ E_z \end{Bmatrix}_{(k)}, \tag{13}$$

where

$$Q_{11(k)} = Q_{22(k)} = \frac{E_n}{1 - \nu_k^2}, \tag{14a}$$

$$Q_{12(k)} = \frac{\nu_k E_k}{1 - \nu_k^2}, \tag{14b}$$

$$Q_{44(k)} = Q_{55(k)} = Q_{66(k)} = \frac{\nu_k E_k}{2(1 + \nu_k)}. \tag{14c}$$

Wang and Wang et al. [58,59] reported that the distribution of the electric potential in the flexural direction is a half-cosine distribution when a uniform moment is applied to the piezoelectric structures. They assumed the electric potential as a combination of a half-cosine and linear variation and verified that this assumption satisfies the Maxwell static electricity equation, namely, the sinusoidal variation of the potential, by using Finite Element Method [58]. The assumed form of the electric potential was also applied by Ke et al. [50] and Liu et al. [51] to study the vibrations of the nonlocal piezoelectric nanoplates. Therefore, the combination distributions of the half-cosine and linear variation on the electric potential are adopted to analyze the vibrations of the GNPL reinforced functionally gradient nonlocal piezoelectric composite microplate

$$\hat{\phi}(x, y, z, t) = -\cos(\beta z)\, \phi(x, y, t) + \frac{2zV_0}{h} \mathrm{e}^{i\Omega t}, \tag{15}$$

where V_0 is the external electric voltage, $\beta = \pi / h$, $\phi(x, y, t)$ and Ω represents respectively the distribution of the electric potential in the mid-plane and the natural frequency of the GNPL reinforced functionally graded piezoelectric composite microplate.

Then the electric fields of the *k*-th GNPL reinforced nonlocal piezoelectric layer are obtained as

$$E_x = -\frac{\partial \hat{\phi}}{\partial x} = \cos(\beta z) \frac{\partial \phi}{\partial x}, \tag{16a}$$

$$E_y = -\frac{\partial \hat{\phi}}{\partial y} = \cos(\beta z) \frac{\partial \phi}{\partial y}, \tag{16b}$$

$$E_z = -\frac{\partial \hat{\phi}}{\partial z} = -\beta \sin(\beta z)\, \phi - \frac{2V_0}{h} \mathrm{e}^{i\Omega t}. \tag{16c}$$

Therefore, the strain energy Π_s of the GNPL reinforced functionally graded piezoelectric composite microplate is expressed as

$$\begin{aligned}
\Pi_s &= \frac{1}{2}\int_A \sum_{n=1}^{N} \int_{z_n}^{z_{n+1}} \left(\sigma_{xx}\varepsilon_{xx} + \sigma_{yy}\varepsilon_{yy} + 2\sigma_{xy}\varepsilon_{xy} + 2\sigma_{xz}\varepsilon_{xz} + 2\sigma_{yz}\varepsilon_{yz}\right)_{(n)} dzdA \\
&\quad - \frac{1}{2}\int_A \sum_{n=1}^{N} \int_{z_n}^{z_{n+1}} \left(D_x E_x + D_y E_y + D_z E_z\right)_{(n)} dzdA \\
&= \frac{1}{2}\int_A \left(N_x \varepsilon_{xx}^{(0)} + N_y \varepsilon_{yy}^{(0)} + 2N_{xy}\varepsilon_{xy}^{(0)} + 2Q_x \varepsilon_{xz}^{(0)} + 2Q_y \varepsilon_{yz}^{(0)} + M_x \varepsilon_{xx}^{(1)} + M_y \varepsilon_{yy}^{(1)} + 2M_{xy}\varepsilon_{xy}^{(1)}\right)_{(n)} dA \\
&\quad - \frac{1}{2}\int_A \sum_{n=1}^{N} \int_{z_n}^{z_{n+1}} \left\{ D_x \cos(\beta z)\frac{\partial \phi}{\partial x} + D_y \cos(\beta z)\frac{\partial \phi}{\partial y} - D_z\left[\beta \sin(\beta z)\phi + \frac{2V_0}{h} e^{i\Omega t}\right]\right\}_{(n)} dzdA,
\end{aligned} \tag{17}$$

where A is the domain of the mid-plane for the GNPL reinforced functionally gradient piezoelectric composite microplate, N_x and N_y are the normal resultants, N_{xy} is the twisting shear force

$$\{N_x, N_y, N_{xy}\} = \sum_{k=1}^{N} \int_{z_k}^{z_{k+1}} [\sigma_{xx}, \sigma_{yy}, \sigma_{xy}]_{(k)} dz \,, \tag{18a}$$

Q_x and Q_y are the shearing forces

$$\{Q_x, Q_y\} = \sum_{k=1}^{N} \int_{z_k}^{z_{k+1}} [\sigma_{xz}, \sigma_{yz}]_{(k)} dz \,, \tag{18b}$$

M_x and M_y are the bending moments, M_{xy} is the twisting moment

$$\{M_x, M_y, M_{xy}\} = \sum_{k=1}^{N} \int_{z_k}^{z_{k+1}} [\sigma_{xx}, \sigma_{yy}, \sigma_{xy}]_{(k)} z dz \,. \tag{18c}$$

The kinetic energy Π_k of the GNPL reinforced functionally gradient piezoelectric composite microplate is calculated by

$$\Pi_k = \frac{1}{2} \int_A (I_1 \dot{U}^2 + I_1 \dot{V}^2 + I_1 \dot{W}^2 + I_3 \dot{\varphi}_x^2 + I_3 \dot{\varphi}_y^2) dA \,, \tag{19}$$

where the inertia terms I_i ($i = 0, 2$) are defined as

$$I_i = \sum_{n=1}^{N} \int_{z_n}^{z_{n+1}} z^i \rho_n dz \,,\ (i = 0, 2). \tag{20}$$

The work done by the Winkler elastic foundation is denoted by Π_F

$$\Pi_F = -\frac{1}{2} \int_A k_l W^2 dA \,, \tag{21}$$

where k_l is the elasticity coefficient of the Winkler elastic foundation.

Based on Hamilton's principle, we have

$$\int_0^t (\delta \Pi_k + \delta \Pi_F - \delta \Pi_s) dt = 0 \,. \tag{22}$$

The nonlinear partial differential governing equations of motion for the GNPL reinforced functionally gradient piezoelectric composite microplate are established as

$$\delta U: \quad \frac{\partial N_x}{\partial x} + \frac{\partial N_{xy}}{\partial y} = I_1 \ddot{U} \,, \tag{23a}$$

$$\delta V: \quad \frac{\partial N_y}{\partial y} + \frac{\partial N_{xy}}{\partial x} = I_1 \ddot{V} \,, \tag{23b}$$

$$\delta W: \quad \frac{\partial}{\partial x}\left(N_x \frac{\partial w}{\partial x} + N_{xy} \frac{\partial w}{\partial y} \right) + \frac{\partial}{\partial y}\left(N_y \frac{\partial w}{\partial y} + N_{xy} \frac{\partial w}{\partial x} \right) + \frac{\partial Q_x}{\partial x} + \frac{\partial Q_y}{\partial y} - k_l W = I_1 \ddot{W} \,, \tag{23c}$$

$$\delta\varphi_x: \qquad \frac{\partial M_x}{\partial x}+\frac{\partial M_{xy}}{\partial y}-Q_x=I_3\ddot{\varphi}_x, \tag{23d}$$

$$\delta\varphi_y: \qquad \frac{\partial M_y}{\partial y}+\frac{\partial M_{xy}}{\partial x}-Q_y=I_3\ddot{\varphi}_y, \tag{23e}$$

$$\delta\phi: \qquad \sum_{n=1}^{N}\int_{z_n}^{z_{n+1}}\left[\frac{\partial D_x}{\partial x}\cos(\beta z)+\frac{\partial D_y}{\partial y}\cos(\beta z)+D_z\beta\sin(\beta z)\right]_{(n)}dz=0. \tag{23f}$$

It is worth noticed that equations (23a)-(23f) are the classical nonlinear partial differential governing equations of motion for the piezoelectric FSDT plates. However, the definitions of the stress resultants are novel here. Substituting the nonlocal constitutive equation (13) into equation (18), the novel stress resultants are yielded as

$$N_x-(e_0a_0)^2\nabla^2N_x=A_{11}\left[\frac{\partial U}{\partial x}+\frac{1}{2}\left(\frac{\partial W}{\partial x}\right)^2\right]+A_{12}\left[\frac{\partial V}{\partial y}+\frac{1}{2}\left(\frac{\partial W}{\partial y}\right)^2\right]-N_{x0}, \tag{24a}$$

$$N_y-(e_0a_0)^2\nabla^2N_y=A_{12}\left[\frac{\partial U}{\partial x}+\frac{1}{2}\left(\frac{\partial W}{\partial x}\right)^2\right]+A_{11}\left[\frac{\partial V}{\partial y}+\frac{1}{2}\left(\frac{\partial W}{\partial y}\right)^2\right]-N_{y0}, \tag{24b}$$

$$N_{xy}-(e_0a_0)^2\nabla^2N_{xy}=A_{66}\left(\frac{\partial U}{\partial y}+\frac{\partial V}{\partial x}+\frac{\partial W}{\partial x}\frac{\partial W}{\partial y}\right), \tag{24c}$$

$$M_x-(e_0a_0)^2\nabla^2M_x=D_{11}\frac{\partial\varphi_x}{\partial x}+D_{12}\frac{\partial\varphi_y}{\partial y}+E_{31}\phi, \tag{24d}$$

$$M_y-(e_0a_0)^2\nabla^2M_y=D_{12}\frac{\partial\varphi_x}{\partial x}+D_{11}\frac{\partial\varphi_y}{\partial y}+E_{31}\phi, \tag{24e}$$

$$M_{xy}-(e_0a_0)^2\nabla^2M_{xy}=D_{66}\left(\frac{\partial\varphi_x}{\partial y}+\frac{\partial\varphi_y}{\partial x}\right), \tag{24f}$$

$$Q_x-(e_0a_0)^2\nabla^2Q_x=k_sA_{44}\left(\frac{\partial W}{\partial x}+\varphi_x\right)-k_sE_{15}\frac{\partial\phi}{\partial x}, \tag{24g}$$

$$Q_y-(e_0a_0)^2\nabla^2Q_y=k_sA_{44}\left(\frac{\partial W}{\partial y}+\varphi_y\right)-k_sE_{24}\frac{\partial\phi}{\partial y}, \tag{24h}$$

$$\sum_{k=1}^{N}\int_{z_k}^{z_{k+1}}\cos(\beta z)\left[D_x-(e_0a_0)^2\nabla^2D_x\right]dz=E_{15}\left(\varphi_x+\frac{\partial W}{\partial x}\right)+X_{11}\frac{\partial\phi}{\partial x}, \tag{24i}$$

$$\sum_{k=1}^{N}\int_{z_k}^{z_{k+1}}\cos(\beta z)\left[D_y-(e_0a_0)^2\nabla^2D_y\right]dz=E_{15}\left(\varphi_y+\frac{\partial W}{\partial y}\right)+X_{11}\frac{\partial\phi}{\partial y}, \tag{24j}$$

$$\sum_{k=1}^{N}\int_{z_k}^{z_{k+1}}\beta\sin(\beta z)\left[D_z-(e_0a_0)^2\nabla^2 D_z\right]dz=E_{31}\frac{\partial\varphi_x}{\partial x}+E_{31}\frac{\partial\varphi_y}{\partial y}-X_{33}\phi\,, \tag{24k}$$

where the shear correction factor $k_s = 5/6$ and

$$\begin{bmatrix} N_{x0} \\ N_{y0} \end{bmatrix}=\begin{bmatrix} -\dfrac{2V_0}{h}\displaystyle\sum_{n=1}^{N}\int_{z_n}^{z_{n+1}} e_{31,k}dz \\ -\dfrac{2V_0}{h}\displaystyle\sum_{n=1}^{N}\int_{z_n}^{z_{n+1}} e_{32,k}dz \end{bmatrix}, \tag{25}$$

the coefficients $[A]$, $[B]$, $[D]$, $[E]$ and $[X]$ are respectively given in the Appendix A.

Combining equations (23) and (24), the novel nonlinear partial differential governing equations of the motion are rewritten for the GNPL reinforced functionally gradient piezoelectric composite microplate

$$A_{11}\left(\frac{\partial^2 U}{\partial x^2}+\frac{\partial W}{\partial x}\frac{\partial^2 W}{\partial x^2}\right)+A_{12}\left(\frac{\partial^2 V}{\partial x\partial y}+\frac{\partial W}{\partial y}\frac{\partial^2 W}{\partial x\partial y}\right)$$
$$+A_{66}\left(\frac{\partial^2 U}{\partial y^2}+\frac{\partial^2 V}{\partial x\partial y}+\frac{\partial W}{\partial y}\frac{\partial^2 W}{\partial x\partial y}+\frac{\partial W}{\partial x}\frac{\partial^2 W}{\partial y^2}\right)=L_{nol}(I_1\ddot{U})\,, \tag{26a}$$

$$A_{12}\left(\frac{\partial^2 U}{\partial x\partial y}+\frac{\partial W}{\partial x}\frac{\partial^2 W}{\partial x\partial y}\right)+A_{22}\left(\frac{\partial^2 U}{\partial y^2}+\frac{\partial W}{\partial y}\frac{\partial^2 W}{\partial y^2}\right)$$
$$+A_{66}\left(\frac{\partial^2 U}{\partial x\partial y}+\frac{\partial^2 V}{\partial x^2}+\frac{\partial W}{\partial y}\frac{\partial^2 W}{\partial x^2}+\frac{\partial W}{\partial x}\frac{\partial^2 W}{\partial x\partial y}\right)=L_{nol}(I_1\ddot{V})\,, \tag{26b}$$

$$Z_1+Z_2-L_{nol}\left(N_{x0}\frac{\partial^2 W}{\partial x^2}-N_{y0}\frac{\partial^2 W}{\partial y^2}\right)+A_{44}\left(\frac{\partial^2 W}{\partial y^2}+\frac{\partial\varphi_y}{\partial y}\right)$$
$$+A_{55}\left(\frac{\partial^2 W}{\partial x^2}+\frac{\partial\varphi_x}{\partial x}\right)-K_s\left(E_{15}\frac{\partial^2\phi}{\partial x^2}+E_{24}\frac{\partial^2\phi}{\partial y^2}\right)-L_{nol}(k_l W)=L_{nol}(I_1\ddot{W})\,, \tag{26c}$$

$$D_{11}\frac{\partial^2\varphi_x}{\partial x^2}+D_{12}\frac{\partial^2\varphi_y}{\partial x\partial y}+D_{66}\left(\frac{\partial^2\varphi_x}{\partial y^2}+\frac{\partial^2\varphi_y}{\partial x\partial y}\right)+E_{31}\frac{\partial\phi}{\partial x}$$
$$-A_{55}\left(\frac{\partial W}{\partial x}+\varphi_x\right)+K_sE_{15}\frac{\partial\phi}{\partial x}=L_{nol}(I_1\ddot{\varphi}_x)\,, \tag{26d}$$

$$D_{12}\frac{\partial^2\varphi_x}{\partial x\partial y}+D_{22}\frac{\partial^2\varphi_y}{\partial y^2}+D_{66}\left(\frac{\partial^2\varphi_x}{\partial x\partial y}+\frac{\partial^2\varphi_y}{\partial x^2}\right)+E_{32}\frac{\partial\phi}{\partial y}$$
$$-A_{44}\left(\frac{\partial W}{\partial y}+\varphi_y\right)+K_sE_{24}\frac{\partial\phi}{\partial y}=L_{nol}(I_1\ddot{\varphi}_y)\,, \tag{26e}$$

$$E_{15}\left(\frac{\partial^2 W}{\partial x^2}+\frac{\partial \varphi_x}{\partial x}\right)+E_{24}\left(\frac{\partial^2 W}{\partial y^2}+\frac{\partial \varphi_y}{\partial y}\right)+E_{31}\frac{\partial \phi}{\partial x}+E_{32}\frac{\partial \phi}{\partial y}$$

$$+X_{11}\frac{\partial^2 \phi}{\partial x^2}+X_{22}\frac{\partial^2 \phi}{\partial y^2}-X_{33}\phi=0\,, \tag{26f}$$

with $L_{nol}=1-\left[(e_0 a_0)^2\nabla^2\right]$ and nonlinear items Z_1 and Z_2 which are given in the Appendix A.

Adopting the following dimensionless parameters, we have

$$\{\zeta,\xi\}=\left\{\frac{x}{a_M},\frac{y}{b_M}\right\},\ \{u,v,w\}=\left\{\frac{U}{h_M},\frac{V}{h_M},\frac{W}{h_M}\right\},\ \eta=\frac{a_M}{h_M},\ \lambda=\frac{a_M}{b_M}, \tag{27a}$$

$$\overline{A}_{ij}=\frac{A_{ij}}{A_{110}},\ \overline{D}_{ij}=\frac{D_{ij}}{A_{110}h_M{}^2},\ \{\overline{I}_1,\overline{I}_3\}=\left\{\frac{I_1}{I_{10}},\frac{I_3}{I_{10}h_M{}^2}\right\}, \tag{27b}$$

$$A_{110}=\frac{E_M}{1-\nu_M^2}h_M,\ I_{10}=\rho_M h_M,\ \mu=\frac{e_0 a_0}{a_M},\ \overline{k}_l=\frac{k_l a_M{}^2}{A_{110}}, \tag{27c}$$

$$\{\overline{X}_{11},\overline{X}_{22},\overline{X}_{33}\}=\left\{\frac{X_{11}\phi_0^2}{A_{110}h_M{}^2},\frac{X_{22}\phi_0^2}{A_{110}h_M{}^2},\frac{X_{33}\phi_0^2}{A_{110}}\right\}, \tag{27d}$$

$$\{\overline{E}_{31},\overline{E}_{32},\overline{E}_{24},\overline{E}_{15}\}=\left\{\frac{E_{31}\phi_0}{A_{110}h_M},\frac{E_{32}\phi_0}{A_{110}h_M},\frac{E_{24}\phi_0}{A_{110}h_M},\frac{E_{15}\phi_0}{A_{110}h_M}\right\}, \tag{27e}$$

$$\{\overline{N}_{x0},\overline{N}_{y0}\}=\left\{\frac{N_{x0}}{A_{110}},\frac{N_{y0}}{A_{110}}\right\},\ \overline{\phi}=\frac{\phi}{\phi_0},\ \phi_0=\sqrt{\frac{A_{110}}{X_{33}}},\ \tau=\frac{t}{a}\sqrt{\frac{A_{110}}{I_{10}}}. \tag{27f}$$

The dimensionless form of the nonlinear partial differential governing equation (25) is illustrated in the Appendix B.

In the present analyses, the electric potential is assumed to be zero at the four edges of the GNPL reinforced functionally graded piezoelectric composite microplate and three distinct boundary conditions are given, including the SSSS, CCCC and CCSS.

The SSSS boundary conditions represent that the GNPL reinforced functionally graded piezoelectric composite microplate is simply supported at the four edges, which are expressed in the dimensionless form

$$u=v=w=\varphi_y=\overline{\phi}=0\,,\ \overline{D}_{11}\frac{\partial \varphi_x}{\partial \zeta}+\lambda\overline{D}_{12}\frac{\partial \varphi_y}{\partial \xi}+\eta\overline{E}_{31}\overline{\phi}=0\,,\ (\zeta=0,1), \tag{28a}$$

$$u=v=w=\varphi_x=\overline{\phi}=0\,,\ \overline{D}_{12}\frac{\partial \varphi_x}{\partial \zeta}+\lambda\overline{D}_{22}\frac{\partial \varphi_y}{\partial \xi}+\eta\overline{E}_{32}\overline{\phi}=0\,,\ (\xi=0,1). \tag{28b}$$

The CCCC boundary conditions denote that the GNPL reinforced functionally graded piezoelectric composite microplate is clamped at the four edges, which are expressed in the dimensionless form

$$u = v = w = \varphi_x = \varphi_y = \overline{\phi} = 0, \; (\zeta = 0,1 \;\; \text{and} \;\; \xi = 0,1). \tag{29}$$

The CCSS boundary conditions demonstrate that the GNPL reinforced functionally graded piezoelectric composite microplate is clamped at two adjacent edges, simply supported at other two adjacent edges, which are expressed in the dimensionless form

$$u = v = w = \varphi_x = \varphi_y = \overline{\phi} = 0, \; (\zeta = 0, \;\; \xi = 0), \tag{30a}$$

$$u = v = w = \varphi_y = \overline{\phi} = 0, \;\; \overline{D}_{11}\frac{\partial \varphi_x}{\partial \zeta} + \lambda \overline{D}_{12}\frac{\partial \varphi_y}{\partial \xi} + \eta \overline{E}_{31}\overline{\phi} = 0, \; (\zeta = 1), \tag{30b}$$

$$u = v = w = \varphi_x = \overline{\phi} = 0, \;\; \overline{D}_{12}\frac{\partial \varphi_x}{\partial \zeta} + \lambda \overline{D}_{22}\frac{\partial \varphi_y}{\partial \xi} + \eta \overline{E}_{32}\overline{\phi} = 0, \; (\xi = 1). \tag{30c}$$

3. Solution Procedure

Except for a few especial cases, the nonlinear partial differential equations of motion can not be solved analytically. Bellman et al. [60] firstly introduced the differential quadrature (DQ) method to transform the nonlinear partial differential equations of motion into a set of algebraic equations or ordinary differential equations. Quan and Chang [61] introduced a Lagrange interpolation polynomial to efficiently and accurately obtain the explicit formulations for calculating the weighting coefficients on the discretization of the first-order and the second-order derivatives in a single domain. Shu [62] further developed some simple algebraic formulations to compute the weighting coefficients in a single domain and multi-domains and applied them into engineering fields. Due to the convenient and flexibility of the DQ method, some excellent results have been reported in a number of application studies [35,36,50,51,63-66].

In this section, we employ the DQ method to discretize the nonlinear partial differential governing equations of motion for the linear and nonlinear vibrations of the GNPL reinforced functionally gradient piezoelectric composite microplate. The unknown displacement components (u, v, w, φ_x, φ_y and $\overline{\phi}$) and the n_1-th and n_2-th partial derivatives with respect to ζ and ξ are discretized in the domain by N_1 and N_2 grid points respectively along the ζ- and ξ- axes

$$\left\{u, v, w, \varphi_x, \varphi_y, \bar{\phi}\right\} = \sum_{m=1}^{N_1}\sum_{n=1}^{N_2} l_m(\zeta) l_n(\xi) \times \left\{u_{mn}(\zeta_m, \xi_n, \tau), v_{mn}(\zeta_m, \xi_n, \tau), w_{mn}(\zeta_m, \xi_n, \tau),\right.$$

$$\left.\varphi_{x,mn}(\zeta_m, \xi_n, \tau), \varphi_{y,mn}(\zeta_m, \xi_n, \tau), \bar{\phi}_{mn}(\zeta_m, \xi_n, \tau)\right\}, \tag{31a}$$

$$\frac{\partial^{n_1}}{\partial \zeta^{n_1}} \frac{\partial^{n_2}}{\partial \xi^{n_2}} \left\{u, v, w, \varphi_x, \varphi_y, \bar{\phi}\right\}\Big|_{\zeta=\zeta_i, \xi=\xi_j} = \sum_{m=1}^{N_1}\sum_{m=2}^{N_2} C_{im}^{(n_1)} C_{jn}^{(n_2)} \times$$

$$\left\{u_{mn}(\zeta_m, \xi_n, \tau), v_{mn}(\zeta_m, \xi_n, \tau), w_{mn}(\zeta_m, \xi_n, \tau), \varphi_{x,mn}(\zeta_m, \xi_n, \tau), \varphi_{y,mn}(\zeta_m, \xi_n, \tau), \bar{\phi}_{mn}(\zeta_m, \xi_n, \tau)\right\}, \tag{31b}$$

where $l_m(\zeta)$ and $l_n(\xi)$ are respectively the Lagrange interpolation polynomials along the ζ - and the ξ -axes, $C_{im}^{n_1}$ and $C_{jn}^{n_2}$ respectively are the corresponding weight coefficients.

For the ζ-axis, the Lagrange interpolation polynomials $l_m(\zeta)$ and the corresponding weight coefficients $C_{im}^{n_1}$ are respectively given as

$$l_m(\zeta) = \frac{\vartheta(\zeta)}{(\zeta - \zeta_m)\vartheta^{(1)}(\zeta)}, \quad \vartheta(\zeta) = \prod_{i=1}^{N_1} (\zeta - \zeta_i), \quad \vartheta^{(1)}(\zeta) = \prod_{i=1, i \neq m}^{N_1} (\zeta_m - \zeta_i), \tag{32a}$$

$$C_{im}^{(1)} = \frac{\vartheta^{(1)}(\zeta_i)}{(\zeta_i - \zeta_m)\vartheta^{(1)}(\zeta_m)}, \ (i, m = 1,2,..., N_1, \ \ i \neq m), \tag{32b}$$

$$C_{im}^{(n_1)} = k\left(C_{ii}^{(n_1-1)} C_{im}^{(1)} - \frac{C_{im}^{(n_1-1)}}{\zeta_i - \zeta_m}\right), \ (i, m = 1,2,..., N_1, i \neq m, \ \ n_1 \geq 2), \tag{32c}$$

$$C_{ii}^{(n_1)} = -\sum_{m=1}^{N_1} C_{im}^{(n_1)}, \ (i, m = 1,2,..., N_1, n_1 \geq 1). \tag{32d}$$

The derivation along the ξ -axis is similar to equation (31), which will not be demonstrated here for brevity. Therefore, the nonlinear partial differential governing equations of motion for the GNPL reinforced functionally gradient nonlocal piezoelectric composite microplate can be represented by a group of nonlinear algebraic expressions

$$\bar{A}_{11}\left(\sum_{m=1}^{N_1} C_{im}^{(2)} u_{mj} + \frac{1}{\eta}\sum_{m=1}^{N_1} C_{im}^{(1)} w_{mj} \sum_{m=1}^{N_1} C_{im}^{(2)} w_{mj}\right)$$

$$+ \bar{A}_{12}\left(\lambda \sum_{m=1}^{N_1}\sum_{n=1}^{N_2} C_{im}^{(1)} C_{jn}^{(1)} v_{mn} + \frac{\lambda^2}{\eta}\sum_{n=1}^{N_2} C_{jn}^{(1)} w_{in} \sum_{m=1}^{N_1}\sum_{n=1}^{N_2} C_{im}^{(1)} C_{jn}^{(1)} w_{mn}\right) + \bar{A}_{66}\left(\lambda^2 \sum_{n=1}^{N_2} C_{jn}^{(2)} u_{in}\right.$$

$$\left. + \lambda \sum_{m=1}^{N_1}\sum_{n=1}^{N_2} C_{im}^{(1)} C_{jn}^{(1)} v_{mn} + \frac{\lambda^2}{\eta}\sum_{n=1}^{N_2} C_{jn}^{(1)} w_{in} \sum_{m=1}^{N_1}\sum_{n=1}^{N_2} C_{im}^{(1)} C_{jn}^{(1)} w_{mn} + \frac{\lambda^2}{\eta}\sum_{m=1}^{N_1} C_{im}^{(1)} w_{mj} \sum_{n=1}^{N_2} C_{jn}^{(2)} w_{in}\right)$$

$$= \bar{I}_1 \ddot{u}_{ij} - \bar{I}_1 \left(\mu^2 \sum_{m=1}^{N_1} C_{im}^{(2)} \ddot{u}_{mj} + \mu^2 \lambda^2 \sum_{n=1}^{N_2} C_{jn}^{(2)} \ddot{u}_{in} \right), \tag{33a}$$

$$\overline{A}_{22} \left(\lambda^2 \sum_{n=1}^{N_2} C_{jn}^{(2)} v_{in} + \frac{\lambda^3}{\eta} \sum_{n=1}^{N_2} C_{jn}^{(1)} w_{in} \sum_{n=1}^{N_2} C_{jn}^{(2)} w_{in} \right)$$

$$+ \overline{A}_{12} \left(\lambda \sum_{m=1}^{N_1} \sum_{n=1}^{N_2} C_{im}^{(1)} C_{jn}^{(1)} u_{mn} + \frac{\lambda}{\eta} \sum_{m=1}^{N_1} C_{im}^{(1)} w_{mj} \sum_{m=1}^{N_1} \sum_{n=1}^{N_2} C_{im}^{(1)} C_{jn}^{(1)} w_{mn} \right) + \overline{A}_{66} \left(\sum_{m=1}^{N_1} C_{im}^{(2)} v_{mj} \right.$$

$$\left. + \lambda \sum_{m=1}^{N_1} \sum_{n=1}^{N_2} C_{im}^{(1)} C_{jn}^{(1)} u_{mn} + \frac{\lambda}{\eta} \sum_{n=1}^{N_2} C_{jn}^{(1)} w_{in} \sum_{m=1}^{N_1} C_{im}^{(2)} w_{mj} + \frac{\lambda}{\eta} \sum_{m=1}^{N_1} C_{im}^{(1)} w_{mj} \sum_{m=1}^{N_1} \sum_{n=1}^{N_2} C_{im}^{(1)} C_{jn}^{(1)} w_{mn} \right)$$

$$= \bar{I}_1 \ddot{v}_{ij} - \bar{I}_1 \left(\mu^2 \sum_{m=1}^{N_1} C_{im}^{(2)} \ddot{v}_{mj} + \mu^2 \lambda^2 \sum_{n=1}^{N_2} C_{jn}^{(2)} \ddot{v}_{in} \right), \tag{33b}$$

$$\overline{Z}_1 + \overline{Z}_2 + \overline{A}_{44} \left(\lambda^2 \sum_{n=1}^{N_2} C_{jn}^{(2)} w_{in} + \lambda \eta \sum_{n=1}^{N_2} C_{jn}^{(1)} \varphi_{y,in} \right) + \overline{A}_{55} \left(\sum_{m=1}^{N_1} C_{im}^{(2)} w_{mj} + \eta \sum_{m=1}^{N_1} C_{im}^{(1)} \varphi_{x,mj} \right)$$

$$- K_s \left(\overline{E}_{15} \sum_{m=1}^{N_1} C_{im}^{(2)} \overline{\phi}_{mj} + \overline{E}_{24} \lambda^2 \sum_{n=1}^{N_2} C_{jn}^{(2)} \overline{\phi}_{in} \right) - \overline{k}_l w_{ij} + \overline{k}_l \left(\mu^2 \sum_{m=1}^{N_1} C_{im}^{(2)} w_{mj} + \mu^2 \lambda^2 \sum_{n=1}^{N_2} C_{jn}^{(2)} w_{in} \right)$$

$$+ \overline{N}_{x0} \left(\mu^2 \sum_{m=1}^{N_1} C_{im}^{(4)} w_{mj} - \sum_{m=1}^{N_1} C_{im}^{(2)} w_{mj} + \mu^2 \lambda^2 \sum_{m=1}^{N_1} \sum_{n=1}^{N_2} C_{im}^{(2)} C_{jn}^{(2)} w_{mn} \right)$$

$$+ \overline{N}_{y0} \lambda^2 \left(\mu^2 \sum_{m=1}^{N_1} \sum_{n=1}^{N_2} C_{im}^{(2)} C_{jn}^{(2)} w_{mn} + \mu^2 \lambda^2 \sum_{n=1}^{N_2} C_{jn}^{(4)} w_{in} - \overline{N}_{y0} \lambda^2 \sum_{n=1}^{N_2} C_{jn}^{(2)} w_{in} \right)$$

$$= \bar{I}_1 \ddot{w}_{ij} - \bar{I}_1 \left(\mu^2 \sum_{m=1}^{N_1} C_{im}^{(2)} \ddot{w}_{mj} + \mu^2 \lambda^2 \sum_{n=1}^{N_2} C_{jn}^{(2)} \ddot{w}_{in} \right), \tag{33c}$$

$$\overline{D}_{11} \sum_{m=1}^{N_1} C_{im}^{(2)} \varphi_{x,mj} + \overline{D}_{12} \lambda \sum_{m=1}^{N_1} \sum_{n=1}^{N_2} C_{im}^{(1)} C_{jn}^{(1)} \varphi_{y,mn} + \overline{D}_{66} \left(\lambda^2 \sum_{n=1}^{N_2} C_{jn}^{(2)} \varphi_{x,in} + \lambda \sum_{m=1}^{N_1} \sum_{n=1}^{N_2} C_{im}^{(1)} C_{jn}^{(1)} \varphi_{y,mn} \right)$$

$$+ \overline{E}_{31} \eta \sum_{m=1}^{N_1} C_{im}^{(1)} \overline{\phi}_{mj} - \overline{A}_{55} \left(\eta \sum_{m=1}^{N_1} C_{im}^{(1)} w_{mj} + \eta^2 \varphi_{x,ij} \right) + K_s \overline{E}_{15} \eta \sum_{m=1}^{N_1} C_{im}^{(1)} \overline{\phi}_{mj}$$

$$= \bar{I}_3 \ddot{\varphi}_{x,ij} - \bar{I}_3 \left(\mu^2 \sum_{m=1}^{N_1} C_{im}^{(2)} \ddot{\varphi}_{x,mj} + \mu^2 \lambda^2 \sum_{n=1}^{N_2} C_{jn}^{(2)} \ddot{\varphi}_{x,in} \right), \tag{33d}$$

$$\overline{D}_{22} \lambda^2 \sum_{n=1}^{N_2} C_{jn}^{(2)} \varphi_{y,in} + \overline{D}_{12} \lambda \sum_{m=1}^{N_1} \sum_{n=1}^{N_2} C_{im}^{(1)} C_{jn}^{(1)} \varphi_{x,mn} + \overline{D}_{66} \left(\sum_{m=1}^{N_1} C_{im}^{(2)} \varphi_{y,mj} + \lambda \sum_{m=1}^{N_1} \sum_{n=1}^{N_2} C_{im}^{(1)} C_{jn}^{(1)} \varphi_{x,mn} \right)$$

$$+\bar{E}_{32}\eta\lambda\sum_{n=1}^{N_2}C_{jn}^{(2)}\bar{\phi}_{in}-\bar{A}_{44}\left(\eta\lambda\sum_{n=1}^{N_2}C_{jn}^{(1)}w_{in}+\eta^2\varphi_{y,ij}\right)+K_s\bar{E}_{24}\eta\lambda\sum_{n=1}^{N_2}C_{jn}^{(1)}\bar{\phi}_{in}$$

$$=\bar{I}_3\ddot{\varphi}_{y,ij}-\bar{I}_3\left(\mu^2\sum_{m=1}^{N_1}C_{im}^{(2)}\ddot{\varphi}_{y,mj}+\mu^2\lambda^2\sum_{n=1}^{N_2}C_{jn}^{(2)}\ddot{\varphi}_{y,in}\right), \tag{33e}$$

$$\bar{E}_{15}\left(\frac{1}{\eta^2}\sum_{m=1}^{N_1}C_{im}^{(2)}w_{mj}+\frac{1}{\eta}\sum_{m=1}^{N_1}C_{im}^{(1)}\varphi_{x,mj}\right)+\bar{E}_{24}\left(\frac{\lambda^2}{\eta^2}\sum_{n=1}^{N_2}C_{jn}^{(2)}w_{in}+\frac{\lambda}{\eta}\sum_{n=1}^{N_2}C_{jn}^{(1)}\varphi_{y,in}\right)$$

$$+\bar{E}_{31}\frac{1}{\eta}\sum_{m=1}^{N_1}C_{im}^{(1)}\bar{\phi}_{mj}+\bar{E}_{32}\frac{\lambda}{\eta}\sum_{n=1}^{N_2}C_{jn}^{(1)}\bar{\phi}_{in}+\bar{X}_{11}\frac{1}{\eta^2}\sum_{m=1}^{N_1}C_{im}^{(2)}\bar{\phi}_{mj}$$

$$+\bar{X}_{22}\frac{\lambda^2}{\eta^2}\sum_{n=1}^{N_2}C_{jn}^{(2)}\bar{\phi}_{in}-\bar{X}_{33}\bar{\phi}_{ij}=0\ , \tag{33f}$$

where the over dots represent the partial derivative with respect to the dimensionless time τ, and the discretized forms of $\bar{Z}_1$ and $\bar{Z}_2$ are rewritten in the Appendix C.

Similarly, the discretized expressions for the boundary conditions in equations (28)-(30) are given in the Appendix D. The matrix form of the differential governing equations for the linear and nonlinear vibrations of the GNPL reinforced functionally gradient nonlocal piezoelectric composite microplate is expressed as

$$\left(\mathbf{K_L}+\mathbf{K_{NL}}\right)\mathbf{d}+\mathbf{M}\,\ddot{\mathbf{d}}=0, \tag{34}$$

$$\mathbf{d}=\left\{\{u_{ij}\}^T,\{v_{ij}\}^T,\{w_{ij}\}^T,\{\varphi_{x,ij}\}^T,\{\varphi_{y,ij}\}^T,\{\phi_{ij}\}^T\right\},\ i=1,2,\cdots,N_1,\ \ j=1,2,\cdots,N_2, \tag{35}$$

where the expressions of the displacement vectors $\{u_{ij}\}$, $\{v_{ij}\}$, $\{w_{ij}\}$, $\{\varphi_{x,ij}\}$, $\{\varphi_{y,ij}\}$, $\{\bar{\phi}_{ij}\}$ are given in the Appendix E, $\mathbf{M}$ is the mass matrix, $\mathbf{K_L}$ and $\mathbf{K_{NL}}$ are respectively the linear and nonlinear stiffness matrices, and $\mathbf{M}$, $\mathbf{K_L}$ and $\mathbf{K_{NL}}$ are all $6N_1N_2\times 6N_1N_2$ matrices.

The dynamic displacement vector $\mathbf{d}$ can be expanded in the form of

$$\mathbf{d}=\mathbf{d}^*\mathrm{e}^{i\omega t}, \tag{36}$$

where $\omega=\Omega a\sqrt{I_{10}/A_{110}}$ is the dimensionless natural frequency of the GNPL reinforced functionally gradient piezoelectric composite microplate, $\mathbf{d}^*$ indicates the vector of the vibration mode shape for the GNPL reinforced functionally gradient piezoelectric composite microplate and $i^2=-1$.

Substituting equation (36) into equation (35) yields the nonlinear eigenvalue equations

$$\left(\mathbf{K_L}+\mathbf{K_{NL}}\right)\mathbf{d}^*-\omega^2 M\,\ddot{\mathbf{d}}^*=0\,. \tag{37}$$

A direct iterative technique [51] is introduced to solve equation (37) for the dimensionless natural frequencies and the relevant mode shapes of the GNPL reinforced functionally gradient nonlocal piezoelectric composite microplate. Neglecting the nonlinear stiffness matrix $\mathbf{K_{NL}}$, the linear eigenvalue and matching eigenvector are obtained. The obtained eigenvector is employed to solve the transverse vibration amplitudes $w_{\max}$ and to calculate the nonlinear stiffness matrix $\mathbf{K_{NL}}$. A new eigenvalue and the related eigenvector are computed by using the eigenvalue equation (37). Repeating the steps to the relative error between the eigenvalues calculated by two consecutive iterations is within 10^{-4}.

4. Numerical Results and Discussions

The numerical results of the linear and nonlinear vibrations are obtained for the GNPL reinforced functionally gradient nonlocal piezoelectric composite microplate subjected to an external voltage in this section. Three different boundary conditions are considered, including SSSS, CCCC and CCSS. Table 1 demonstrates the piezoelectric capabilities of the PVDF. The effects of the nonlocal coefficient μ, elasticity coefficient k_l of the Winkler elastic foundation, external electric voltage V_0, total layers N and properties of the GNPL reinforcements, including α, V_{gpl} and a_{gpl}/h_{gpl}, on the linear and nonlinear frequencies of the GNPL reinforced functionally gradient piezoelectric composite microplate are analyzed in detail.

Unless otherwise stating, the geometrical characteristics of the GNPL reinforced functionally gradient piezoelectric composite microplate are respectively $h_M=5\ \mu\text{m}$ and $a_M=b_M=50\ \mu\text{m}$. The rectangular GNPL reinforcement has the length a_{gpl}= 5 nm, width b_{gpl}= 2.5 nm and thickness h_{gpl}= 0.3 nm. The GNPL volume fraction is $V_{gpl}=1.0\%$, the nonlocal coefficient is $\mu=0.1$, the piezoelectric multiFple [35,36] is $\alpha=100\times10^3$ and the external voltage V_0 is assumed to be zero. In addition, the elastic properties of the GNPL nanofillers and PVDF are respectively [5,36]

$$E_G=1010\,\text{GPa}\,,\ \ \nu_G=0.186,\ \ \rho_G=1062.5kg/m^3\,,$$

$$E_M=1.44\,\text{GPa}\,,\ \ \nu_M=0.290,\ \ \rho_M=1920.0kg/m^3\,.$$

Setting the number of discrete points to be N_1 and N_2 along the ζ- axis and ξ-axis, which equal to the same value of N_0, the convergence of the DQ method is checked in Table 2. The dimensionless nonlinear frequency ratios ω_{nl} / ω_l of the X pattern composite microplate under CCCC boundary conditions are listed with different vibration amplitude $w_{\max} / h_M$. Obviously, the results tend to converge when $N_0 \geq 13$. To ensure the accuracy and the efficiency of the calculation simultaneously, we select $N_0 = 13$ in the following analyses.

Because there are no available literature to discuss the linear and nonlinear dynamic behaviors of the GNPL reinforced functionally gradient nonlocal piezoelectric micro- and nano- plate, we reduce our research works to the vibrations of the nonlocal PVDF composite microplate and macroscopic GNPL reinforced functionally gradient piezoelectric plate to validate our method and results. Table 3 lists the comparisons of the dimensionless linear frequencies for a nonlocal piezoelectric composite microplate [50] with different geometric parameters and different nonlocal parameters under SSSS boundary conditions. Table 4 gives the influence of the nonlocal parameters on the nonlinear frequency ratios ω_{nl} / ω_l of a lead zirconium titanate (PZT-4) microplate, which was also reported by Liu et al. [51]. Table 5 provides the dimensionless nonlinear frequencies of a macroscopic GNPL reinforced functionally gradient piezoelectric plate with different GNPL volume fractions under CCCC boundary conditions, and gives a comparison with Mao et al.'s results [35]. It is illustrated that the present solutions have a great agreement with the currently other results.

Figure 3 plots the effects of the total number *N* for the GNPL reinforced piezoelectric layers on (a) the dimensionless linear vibration frequency ω_l and (b) the dimensionless nonlinear vibration frequency ω_{nl} of the GNPL reinforced functionally gradient piezoelectric composite microplate under different boundary conditions and different GNPL distribution patterns. For the U pattern, ω_l and ω_{nl} are independent of the total number *N*. It is because the U pattern GNPL reinforced piezoelectric microplate is homogeneous, which is independent to the total number *N*. However, the total number *N* has significant influences on the dimensionless linear vibration frequency and nonlinear vibration frequency of the X and O pattern microplates in which the difference between the GNPLs distributing in the middle layers and the GNPLs distributing in the top and bottom layers increases with the increasing total number *N*. In the X pattern, with the increasing total number *N*, more GNPLs are distributed in the top and bottom layers, which is better for increasing the vibration frequencies [16]. In the O pattern, with the increasing total number N, more GNPLs are distributed in the middle layers, which reduces the stiffness of the microplate [16]. Moreover, for a fixed total volume fraction V_{gpl}, the difference becomes smaller with the increasing total number N, especially when the total number is $N \geq 10$. Hence, both ω_l and ω_{nl} increase distinctly first and then grow slowly for the X pattern. However, both ω_l and ω_{nl} decrease significantly first and then decrease lightly for the O pattern. As a result, both ω_l and ω_{nl} nearly remain unchanged in the X and O patterns when the total number is $N \geq 10$. In the following analysis, we use the total number $N = 10$. For different boundary conditions, it is seen that the GNPL reinforced functionally gradient piezoelectric composite microplates with CCCC boundary conditions have the highest ω_l and ω_{nl} followed by the CCSS and SSSS boundary conditions.

Figure 4 gives the effect of the GNPLs piezoelectric multiple α on the dimensionless linear vibration frequency ω_l for the GNPL reinforced functionally gradient piezoelectric composite microplate under different boundary conditions and different GNPL distribution patterns. Increasing the GNPLs piezoelectric multiple α leads to an increase of the dimensionless linear vibration frequency ω_l for all different kinds of GNPL distributions and boundary conditions. As same as Figure 3, the GNPL reinforced piezoelectric composite microplate with the CCCC boundary conditions have the highest ω_l among all different kinds of boundary conditions.

In Figure 5, only the CCCC boundary conditions are considered to examine the influence of the nonlocal coefficients μ on the dimensionless linear frequency ω_l for the GNPL reinforced functionally gradient piezoelectric composite microplate. For a certain GNPL distribution form, ω_l declines gradually with the increasing nonlocal coefficients μ. In the X pattern, for instance, ω_l decrease from around 1.35 to 0.98 when μ increase from 0 to 0.2. It is proved that ignoring the nonlocal effect may cause the errors or faults for researching the vibration behaviors of the GNPL reinforced functionally gradient piezoelectric composite microplate. As discussed above, the GNPL reinforced functionally gradient piezoelectric composite microplate with the X pattern has the biggest dimensionless linear frequency. The dimensionless linear frequency of the GNPL reinforced functionally gradient piezoelectric composite microplate with the U pattern is bigger than that of the microplate with the O pattern. For the sake of brevity, only the GNPL reinforced functionally gradient piezoelectric composite microplate under the CCCC boundary conditions with the optimum pattern, for example the X Pattern, is considered in the next studies.

The effects of the elastic coefficient k_l of the Winkler elastic foundation on the dimensionless linear frequency ω_l for the GNPL reinforced functionally gradient piezoelectric composite microplates are shown in Figures 6 and 7 respectively with different nonlocal coefficients ($\mu = 0.00$, 0.05 and 0.10) and different GNPL volume fractions ($V_{gpl} = 0.0\%$, 0.5% and 1.0%). On the one hand, for a certain μ and a certain V_{gpl}, the dimensionless linear frequency ω_l increases with the increasing k_l since the increasing k_l implies the enhancement of the system stiffness. On the other hand, for a certain k_l, the dimensionless linear frequency ω_l decreases with the increasing nonlocal coefficients μ but increases with the increasing GNPL volume fractions V_{gpl}.

The effects of the length-to-thickness ratio a_{gpl} / h_{gpl} of the GNPL nanofillers on the dimensionless linear frequency ω_l for the GNPL reinforced functionally gradient piezoelectric composite microplates are represented in Figures 8 and 9 respectively with different nonlocal coefficients ($\mu = 0.00$, 0.05 and 0.10) and different GNPL volume fractions ($V_{gpl} = 0.0\%$, 0.5% and 1.0%). As expected, the dimensionless linear frequency ω_l increases with the decreasing nonlocal coefficients μ and the increasing GNPL volume fractions V_{gpl}. Moreover, the dimensionless linear frequency ω_l increases with increasing the length-to-thickness ratio a_{gpl} / h_{gpl}. The same phenomenon has been found in the macroscopical GNPL reinforced functionally gradient piezoelectric plate [35]. The GNPLs with the thinner thickness and the larger surface are better for improving the vibration responses of the GNPL reinforced functionally gradient piezoelectric composite microplate.

Figure 10 manifests the influence of the external voltage V_0 on the dimensionless linear frequency ω_l for the GNPL reinforced functionally gradient piezoelectric composite microplate with varying GNPLs piezoelectric multiples α. On the one hand, the dimensionless linear frequency ω_l increases with the increasing GNPL piezoelectric multiples α. On the other hand, the negative and positive external voltages can respectively decrease and increase the linear dimensionless linear frequency ω_l.

Figure 11 illustrates the effect of the external voltage V_0 on the nonlinear frequency ratio ω_{nl} / ω_l for the GNPL reinforced functionally gradient piezoelectric composite microplates with varying GNPL piezoelectric multiples α. It is seen that the nonlinear frequency ratio ω_{nl} / ω_l decreases with increasing GNPL piezoelectric multiples α.

Figure 12 presents the influence of the GNPLs piezoelectric multiple α on the nonlinear frequency ratio ω_{nl} / ω_l for the GNPL reinforced functionally gradient piezoelectric composite microplate with the vibration amplitude $w_{\max} / h$ = 0.4 and different nonlocal coefficients ($\mu = 0.00$, 0.05 and 0.10). It can be seen that the nonlinear frequency ratio ω_{nl} / ω_l decreases with increasing the GNPL piezoelectric multiple α for a given nonlocal coefficient μ. However, for a certain GNPL piezoelectric multiple α, the nonlinear frequency ratio ω_{nl} / ω_l is not monotonously increasing or decreasing with increasing the nonlocal coefficients μ. There is a critical range of the GNPL piezoelectric multiple α, below which the nonlinear frequency ratio ω_{nl} / ω_l increases with increasing the nonlocal coefficients μ, upon which ω_{nl} / ω_l decreases with increasing the nonlocal coefficients μ. It is because the small size effect is different with varying GNPL piezoelectric multiples α, which represents the piezoelectric characteristics of the GNPLs.

Figures 13-16 respectively illustrate the effects of the nonlocal coefficients μ, the GNPL volume fractions V_{gpl}, the elastic coefficient k_l of the Winkler elastic foundation and the GNPL length-to-thickness ratio a_{gpl} / h_{gpl} on the nonlinear frequency ratio ω_{nl} / ω_l for the GNPL reinforced functionally gradient piezoelectric composite microplate. For all of these situations, the nonlinear frequency ratio ω_{nl} / ω_l rises with growing vibration amplitude $w_{\max} / h$ when the hard spring exists for the system. Furthermore, the nonlinear frequency ratio ω_{nl} / ω_l decreases with the growth of the nonlocal coefficients μ, GNPL volume fractions V_{gpl} and elastic coefficient k_l of the Winkler elastic foundation, and increases with the improvement of the length-to-thickness ratio a_{gpl} / h_{gpl}. Meanwhile, it is observed in Figure 16 that the influence of the length-to-thickness ratio a_{gpl} / h_{gpl} on the nonlinear frequency ratio ω_{nl} / ω_l becomes smaller when the length-to-thickness ratio increases.

5. Conclusions

This paper investigates the linear and nonlinear vibrations of the GNPL reinforced functionally gradient piezoelectric composite microplate which is resting on the Winkler elastic foundation and subjected to an external voltage in the framework of the nonlocal constitutive relation, von Karman geometric nonlinearity and Hamilton's principle. The modified parallel model Halpin Tsai and the rule of mixture are respectively used to calculate the effective Young's modulus and other elastic and piezoelectric properties of the microplate respectively. Three varying distribution forms of the GNPLs are considered in the GNPL reinforced functionally gradient piezoelectric composite microplate. The DQ method and iteration progress are numerically employed to investigate the small size effect as well as the influences of the external voltage, the physical and geometrical characteristics of the GNPLs and the elasticity coefficient of the Winkler elastic foundation on the vibration responses of the GNPL reinforced functionally gradient piezoelectric composite microplate under various boundary conditions. The results demonstrate that the small size effect cannot be ignored when we investigate the vibration behaviors of the GNPL reinforced functionally gradient piezoelectric composite microplate. Some conclusions are given.

(1) The X Pattern is the optimum distribution form for enhancing the stiffness of the GNPL reinforced functionally gradient piezoelectric composite microplate. The influence of the piezoelectric multiple for the GNPL reinforced functionally gradient piezoelectric composite microplate on the nonlinear frequency ratio is much depended on the small size effect.

(2) The nonlocal coefficients can not only effect the linear and nonlinear vibration characteristics of the GNPL reinforced functionally gradient piezoelectric composite microplate significantly, but also can ignore which terms introducing some errors or faults for researching the vibration of the microplate.

(3) Both increasing the external voltage and the elastic coefficient of the Winkler elastic foundation can improve the stiffness of the GNPL reinforced functionally gradient piezoelectric composite microplate.

(4) The research results also manifest that the GNPLs have great potential value for promoting the applications of the GNPL reinforced functionally gradient piezoelectric composite microplate.

Acknowledgements

The authors gratefully acknowledge the support of National Natural Science Foundation of China (NNSFC) through Grant Nos. 11802005, 11832002 and 11427801, the Funding Project for Academic Human Resources Development in Institutions of Higher Learning under the Jurisdiction of Beijing Municipality (PHRIHLB).

Conflict of Interest Statement

The authors declare that there is no conflict of interests regarding the publication of this paper.

Appendix A

The coefficients in equation (24) are respectively given as

$$\left(A_{ij}, D_{ij}\right) = \sum_{k=1}^{N} \int_{z_k}^{z_{k+1}} \left(1, z^2\right) Q_{ij(k)} dz \ , \ \left(i, j = 1,2,6\right), \ A_{ij} = K_s \sum_{k=1}^{N} \int_{z_k}^{z_{k+1}} Q_{ij(k)} dz \, , \ \left(i, j = 4,5\right),$$

$$E_{31} = \sum_{k=1}^{N} \int_{z_k}^{z_{k+1}} e_{31,k} \beta z \sin\left(\beta z\right) dz \, , \ E_{32} = \sum_{k=1}^{N} \int_{z_k}^{z_{k+1}} e_{32,k} \beta z \sin\left(\beta z\right) dz \, , \ E_{24} = \sum_{k=1}^{N} \int_{z_k}^{z_{k+1}} e_{24,k} \cos\left(\beta z\right) dz \, ,$$

$$E_{15} = \sum_{k=1}^{N} \int_{z_k}^{z_{k+1}} e_{15,k} \cos\left(\beta z\right) dz \, , \ X_{11} = \sum_{k=1}^{N} \int_{z_k}^{z_{k+1}} \kappa_{11,k} \cos^2\left(\beta z\right) dz \, ,$$

$$X_{33} = \sum_{k=1}^{N} \int_{z_k}^{z_{k+1}} \kappa_{33,k} \beta^2 \sin^2\left(\beta z\right) dz \, . \tag{A1}$$

The nonlinear terms Z_1 and Z_2 in equation (26) are given as

$$Z_1 = \left\{ A_{11} \left[\frac{\partial^2 U}{\partial x^2} + \frac{\partial W}{\partial x} \frac{\partial^2 W}{\partial x^2} \right] + A_{12} \left[\frac{\partial^2 V}{\partial x \partial y} + \frac{\partial W}{\partial y} \frac{\partial^2 W}{\partial x \partial y} \right] \right\} L_{nol} \left(\frac{\partial W}{\partial x} \right)$$

$$+ \left\{ A_{11} \left[\frac{\partial U}{\partial x} + \frac{1}{2} \left(\frac{\partial W}{\partial x} \right)^2 \right] + A_{12} \left[\frac{\partial V}{\partial y} + \frac{1}{2} \left(\frac{\partial W}{\partial y} \right)^2 \right] \right\} L_{nol} \left(\frac{\partial^2 W}{\partial x^2} \right)$$

$$+ \left\{ A_{12} \left[\frac{\partial^2 U}{\partial x \partial y} + \frac{\partial W}{\partial x} \frac{\partial^2 W}{\partial x \partial y} \right] + A_{22} \left[\frac{\partial^2 V}{\partial y^2} + \frac{\partial W}{\partial y} \frac{\partial^2 W}{\partial y^2} \right] \right\} L_{nol} \left(\frac{\partial W}{\partial y} \right)$$

$$
+\left\{A_{12}\left[\frac{\partial U}{\partial x}+\frac{1}{2}\left(\frac{\partial W}{\partial x}\right)^2\right]+A_{22}\left[\frac{\partial V}{\partial y}+\frac{1}{2}\left(\frac{\partial W}{\partial y}\right)^2\right]\right\}L_{nol}\left(\frac{\partial^2 W}{\partial y^2}\right),
$$

$$
Z_2 = A_{66}\left(\frac{\partial^2 U}{\partial x\partial y}+\frac{\partial^2 V}{\partial x^2}+\frac{\partial W}{\partial y}\frac{\partial^2 W}{\partial x^2}+\frac{\partial W}{\partial x}\frac{\partial^2 W}{\partial x\partial y}\right)L_{nol}\left(\frac{\partial W}{\partial y}\right)
$$

$$
+A_{66}\left(\frac{\partial^2 U}{\partial y^2}+\frac{\partial^2 V}{\partial x\partial y}+\frac{\partial W}{\partial y}\frac{\partial^2 W}{\partial x\partial y}+\frac{\partial W}{\partial x}\frac{\partial^2 W}{\partial y^2}\right)L_{nol}\left(\frac{\partial W}{\partial x}\right)
$$

$$
+2A_{66}\left(\frac{\partial U}{\partial y}+\frac{\partial V}{\partial x}+\frac{\partial W}{\partial x}\frac{\partial W}{\partial y}\right)L_{nol}\left(\frac{\partial^2 W}{\partial x\partial y}\right). \tag{A2}
$$

Appendix B

The dimensionless forms of the nonlinear partial differential equation (26) are given as

$$
\overline{A}_{11}\left(\frac{\partial^2 u}{\partial\zeta^2}+\frac{1}{\eta}\frac{\partial w}{\partial\zeta}\frac{\partial^2 w}{\partial\zeta^2}\right)+\overline{A}_{12}\left(\lambda\frac{\partial^2 v}{\partial\zeta\partial\xi}+\frac{\lambda^2}{\eta}\frac{\partial w}{\partial\xi}\frac{\partial^2 w}{\partial\zeta\partial\xi}\right)
$$

$$
+\overline{A}_{66}\left(\lambda^2\frac{\partial^2 u}{\partial\xi^2}+\lambda\frac{\partial^2 v}{\partial\zeta\partial\xi}+\frac{\lambda^2}{\eta}\frac{\partial w}{\partial\xi}\frac{\partial^2 w}{\partial\zeta\partial\xi}+\frac{\lambda^2}{\eta}\frac{\partial w}{\partial\zeta}\frac{\partial^2 w}{\partial\xi^2}\right)=\overline{L}_{nol}(\overline{I}_1\ddot{u}),
$$

$$
\overline{A}_{12}\left(\lambda\frac{\partial^2 u}{\partial\zeta\partial\xi}+\frac{\lambda}{\eta}\frac{\partial w}{\partial\zeta}\frac{\partial^2 w}{\partial\zeta\partial\xi}\right)+\overline{A}_{22}\left(\lambda^2\frac{\partial^2 u}{\partial\xi^2}+\frac{\lambda^3}{\eta}\frac{\partial w}{\partial\xi}\frac{\partial^2 w}{\partial\xi^2}\right)
$$

$$
+\overline{A}_{66}\left(\lambda\frac{\partial^2 u}{\partial\zeta\partial\xi}+\lambda\frac{\partial^2 v}{\partial\zeta^2}+\frac{\lambda}{\eta}\frac{\partial w}{\partial\xi}\frac{\partial^2 w}{\partial\zeta^2}+\frac{\lambda}{\eta}\frac{\partial w}{\partial\zeta}\frac{\partial^2 w}{\partial\zeta\partial\xi}\right)=\overline{L}_{nol}(\overline{I}_1\ddot{v}),
$$

$$
\overline{Z}_1+\overline{Z}_2-\overline{L}_{nol}\left(\overline{N}_{x0}\frac{\partial^2 w}{\partial\zeta^2}+\overline{N}_{y0}\lambda^2\frac{\partial^2 w}{\partial\xi^2}\right)-\overline{L}_{nol}\left(\overline{k}_l w\right)+\overline{A}_{44}\left(\lambda^2\frac{\partial^2 w}{\partial\xi^2}+\lambda\eta\frac{\partial\varphi_y}{\partial\xi}\right)
$$

$$
+\overline{A}_{55}\left(\frac{\partial^2 w}{\partial\zeta^2}+\eta\frac{\partial\varphi_x}{\partial\zeta}\right)-K_s\left(\overline{E}_{15}\frac{\partial^2\overline{\phi}}{\partial\zeta^2}+\overline{E}_{24}\lambda^2\frac{\partial^2\overline{\phi}}{\partial\xi^2}\right)=\overline{L}_{nol}(\overline{I}_1\ddot{w}),
$$

$$
\overline{D}_{11}\frac{\partial^2\varphi_x}{\partial\zeta^2}+\overline{D}_{12}\lambda\frac{\partial^2\varphi_y}{\partial\zeta\partial\xi}+\overline{D}_{66}\left(\lambda^2\frac{\partial^2\varphi_x}{\partial\xi^2}+\lambda\frac{\partial^2\varphi_y}{\partial\zeta\partial\xi}\right)+\overline{E}_{15}\eta\frac{\partial\overline{\phi}}{\partial\zeta}
$$

$$
-\overline{A}_{55}\left(\eta\frac{\partial w}{\partial\zeta}+\eta^2\varphi_x\right)+K_s\overline{E}_{15}\eta\frac{\partial\overline{\phi}}{\partial\zeta}=\overline{L}_{nol}\left(\overline{I}_3\ddot{\varphi}_x\right),
$$

$$
\overline{D}_{12}\lambda\frac{\partial^2\varphi_x}{\partial\zeta\partial\xi}+\overline{D}_{22}\lambda^2\frac{\partial^2\varphi_y}{\partial\xi^2}+\overline{D}_{66}\left(\lambda\frac{\partial^2\varphi_x}{\partial\zeta\partial\xi}+\frac{\partial^2\varphi_y}{\partial\zeta^2}\right)+\overline{E}_{32}\eta\lambda\frac{\partial\overline{\phi}}{\partial\xi}
$$

$$-\overline{A}_{44}\left(\eta\lambda\frac{\partial w}{\partial\xi}+\eta^2\varphi_y\right)+K_s\overline{E}_{24}\eta\lambda\frac{\partial\overline{\phi}}{\partial\xi}=\overline{L}_{nol}\left(\bar{I}_3\ddot{\varphi}_y\right),$$

$$\overline{E}_{15}\left(\frac{1}{\eta^2}\frac{\partial^2 w}{\partial\zeta^2}+\frac{1}{\eta}\frac{\partial\varphi_x}{\partial\zeta}\right)+\overline{E}_{24}\left(\frac{\lambda^2}{\eta^2}\frac{\partial^2 w}{\partial\xi^2}+\frac{\lambda}{\eta}\frac{\partial\varphi_y}{\partial\xi}\right)+\overline{E}_{31}\frac{1}{\eta}\frac{\partial\overline{\phi}}{\partial\zeta}+\overline{E}_{32}\frac{\lambda}{\eta}\frac{\partial\overline{\phi}}{\partial\xi}$$

$$+\overline{X}_{11}\frac{1}{\eta^2}\frac{\partial^2\overline{\phi}}{\partial\zeta^2}+\overline{X}_{22}\frac{\lambda^2}{\eta^2}\frac{\partial^2\overline{\phi}}{\partial\xi^2}-\overline{X}_{33}\overline{\phi}=0\,, \qquad \text{(B1)}$$

where

$$\overline{Z}_1=\left\{\overline{A}_{11}\left[\frac{1}{\eta}\frac{\partial^2 u}{\partial\zeta^2}+\frac{1}{\eta^2}\frac{\partial w}{\partial\zeta}\frac{\partial^2 w}{\partial\zeta^2}\right]+\overline{A}_{12}\left[\frac{\lambda}{\eta}\frac{\partial^2 v}{\partial\zeta\partial\xi}+\frac{\lambda^2}{\eta^2}\frac{\partial w}{\partial\xi}\frac{\partial^2 w}{\partial\zeta\partial\xi}\right]\right\}\overline{L}_{nol}\left(\frac{\partial w}{\partial\zeta}\right)$$

$$+\left\{\overline{A}_{11}\left[\frac{1}{\eta}\frac{\partial u}{\partial\zeta}+\frac{1}{2\eta^2}\left(\frac{\partial w}{\partial\zeta}\right)^2\right]+\overline{A}_{12}\left[\frac{\lambda}{\eta}\frac{\partial v}{\partial\xi}+\frac{\lambda^2}{2\eta^2}\left(\frac{\partial w}{\partial\xi}\right)^2\right]\right\}\overline{L}_{nol}\left(\frac{\partial^2 w}{\partial\zeta^2}\right)$$

$$+\left\{\overline{A}_{12}\left[\frac{\lambda}{\eta}\frac{\partial^2 u}{\partial\zeta\partial\xi}+\frac{\lambda}{\eta^2}\frac{\partial w}{\partial\zeta}\frac{\partial^2 w}{\partial\zeta\partial\xi}\right]+\overline{A}_{22}\left[\frac{\lambda^2}{\eta}\frac{\partial^2 v}{\partial\xi^2}+\frac{\lambda^3}{\eta^2}\frac{\partial w}{\partial\xi}\frac{\partial^2 w}{\partial\xi^2}\right]\right\}\lambda\overline{L}_{nol}\left(\frac{\partial w}{\partial\xi}\right)$$

$$+\left\{\overline{A}_{12}\left[\frac{1}{\eta}\frac{\partial u}{\partial\zeta}+\frac{1}{2\eta^2}\left(\frac{\partial w}{\partial\zeta}\right)^2\right]+\overline{A}_{22}\left[\frac{\lambda}{\eta}\frac{\partial v}{\partial\xi}+\frac{\lambda^2}{2\eta^2}\left(\frac{\partial w}{\partial\xi}\right)^2\right]\right\}\lambda^2\overline{L}_{nol}\left(\frac{\partial^2 w}{\partial\xi^2}\right),$$

$$\overline{Z}_2=\overline{A}_{66}\left(\frac{\lambda}{\eta}\frac{\partial^2 u}{\partial\zeta\partial\xi}+\frac{1}{\eta}\frac{\partial^2 v}{\partial\zeta^2}+\frac{\lambda}{\eta^2}\frac{\partial w}{\partial\xi}\frac{\partial^2 w}{\partial\zeta^2}+\frac{\lambda}{\eta^2}\frac{\partial w}{\partial\zeta}\frac{\partial^2 w}{\partial\zeta\partial\xi}\right)\lambda\overline{L}_{nol}\left(\frac{\partial w}{\partial\xi}\right)$$

$$+\overline{A}_{66}\left(\frac{\lambda^2}{\eta}\frac{\partial^2 u}{\partial\xi^2}+\frac{\lambda}{\eta}\frac{\partial^2 v}{\partial\zeta\partial\xi}+\frac{\lambda^2}{\eta^2}\frac{\partial w}{\partial\xi}\frac{\partial^2 w}{\partial\zeta\partial\xi}+\frac{\lambda^2}{\eta^2}\frac{\partial w}{\partial\zeta}\frac{\partial^2 w}{\partial\xi^2}\right)\overline{L}_{nol}\left(\frac{\partial w}{\partial\zeta}\right)$$

$$+2\overline{A}_{66}\left(\frac{\lambda}{\eta}\frac{\partial u}{\partial\xi}+\frac{1}{\eta}\frac{\partial v}{\partial\zeta}+\frac{\lambda}{\eta^2}\frac{\partial w}{\partial\zeta}\frac{\partial w}{\partial\xi}\right)\lambda\overline{L}_{nol}\left(\frac{\partial^2 w}{\partial\zeta\partial\xi}\right),$$

$$\overline{L}_{nol}=\left[1-\mu^2\left(\frac{\partial^2}{\partial\zeta^2}+\lambda^2\frac{\partial^2}{\partial\xi^2}\right)\right]. \qquad \text{(B2)}$$

Appendix C

The discretized forms of $\overline{Z}_1$ and $\overline{Z}_2$ in equation (33) are rewritten as

$$\overline{Z}_1=\overline{A}_{11}\left(\frac{1}{\eta}\sum_{m=1}^{N_1}C_{im}^{(2)}u_{mj}+\frac{1}{\eta^2}\sum_{m=1}^{N_1}C_{im}^{(1)}w_{mj}\times\sum_{m=1}^{N_1}C_{im}^{(2)}w_{mj}\right)$$

$$\times\left[\sum_{m=1}^{N_1} C_{im}^{(1)} w_{mj} - \left(\mu^2 \sum_{m=1}^{N_1} C_{im}^{(3)} w_{mj} + \mu^2\lambda^2 \sum_{m=1}^{N_1}\sum_{n=1}^{N_2} C_{im}^{(1)} C_{jn}^{(2)} w_{mn}\right)\right]$$

$$+\overline{A}_{12}\left(\frac{\lambda}{\eta}\sum_{m=1}^{N_1}\sum_{n=1}^{N_2} C_{im}^{(1)} C_{jn}^{(1)} v_{mn} + \frac{\lambda^2}{\eta^2}\sum_{n=1}^{N_2} C_{jn}^{(1)} w_{in} \sum_{m=1}^{N_1}\sum_{n=1}^{N_2} C_{im}^{(1)} C_{jn}^{(1)} w_{mn}\right)$$

$$\times\left[\sum_{m=1}^{N_1} C_{im}^{(1)} w_{mj} - \left(\mu^2 \sum_{m=1}^{N_1} C_{im}^{(3)} w_{mj} + \mu^2\lambda^2 \sum_{m=1}^{N_1}\sum_{n=1}^{N_2} C_{im}^{(1)} C_{jn}^{(2)} w_{mn}\right)\right]$$

$$+\overline{A}_{11}\left[\frac{1}{\eta}\sum_{m=1}^{N_1} C_{im}^{(1)} u_{mj} + \frac{1}{2\eta^2}\left(\sum_{m=1}^{N_1} C_{im}^{(1)} w_{mj}\right)^2\right]$$

$$\times\left[\sum_{m=1}^{N_1} C_{im}^{(2)} w_{mj} - \left(\mu^2 \sum_{m=1}^{N_1} C_{im}^{(4)} w_{mj} + \mu^2\lambda^2 \sum_{m=1}^{N_1}\sum_{n=1}^{N_2} C_{im}^{(2)} C_{jn}^{(2)} w_{mn}\right)\right]$$

$$+\overline{A}_{12}\left[\frac{\lambda}{\eta}\sum_{n=1}^{N_2} C_{jn}^{(1)} v_{in} + \frac{\lambda^2}{2\eta^2}\left(\sum_{n=1}^{N_2} C_{jn}^{(1)} w_{in}\right)^2\right]$$

$$\times\left[\sum_{m=1}^{N_1} C_{im}^{(2)} w_{mj} - \left(\mu^2 \sum_{m=1}^{N_1} C_{im}^{(4)} w_{mj} + \mu^2\lambda^2 \sum_{m=1}^{N_1}\sum_{n=1}^{N_2} C_{im}^{(2)} C_{jn}^{(2)} w_{mn}\right)\right]$$

$$+\overline{A}_{12}\left(\frac{\lambda}{\eta}\sum_{m=1}^{N_1}\sum_{n=1}^{N_2} C_{im}^{(1)} C_{jn}^{(1)} u_{mn} + \frac{\lambda}{\eta^2}\sum_{m=1}^{N_1} C_{im}^{(1)} w_{mj} \sum_{m=1}^{N_1}\sum_{n=1}^{N_2} C_{im}^{(1)} C_{jn}^{(1)} w_{mn}\right)$$

$$\times\lambda\left[\sum_{n=1}^{N_2} C_{jn}^{(1)} w_{in} - \left(\mu^2 \sum_{m=1}^{N_1}\sum_{n=1}^{N_2} C_{im}^{(2)} C_{jn}^{(1)} w_{mn} + \mu^2\lambda^2 \sum_{n=1}^{N_2} C_{jn}^{(3)} w_{in}\right)\right]$$

$$+\overline{A}_{22}\left(\frac{\lambda^2}{\eta}\sum_{n=1}^{N_2} C_{jn}^{(2)} v_{in} + \frac{\lambda^3}{\eta^2}\sum_{n=1}^{N_2} C_{jn}^{(1)} w_{in} \times \sum_{n=1}^{N_2} C_{jn}^{(2)} w_{in}\right)$$

$$\times\lambda\left[\sum_{n=1}^{N_2} C_{jn}^{(1)} w_{in} - \left(\mu^2 \sum_{m=1}^{N_1}\sum_{n=1}^{N_2} C_{im}^{(2)} C_{jn}^{(1)} w_{mn} + \mu^2\lambda^2 \sum_{n=1}^{N_2} C_{jn}^{(3)} w_{in}\right)\right]$$

$$+\overline{A}_{12}\left[\frac{1}{\eta}\sum_{m=1}^{N_1} C_{im}^{(1)} u_{mj} + \frac{1}{2\eta^2}\left(\sum_{m=1}^{N_1} C_{im}^{(1)} w_{mj}\right)^2\right]$$

$$\times\lambda^2\left[\sum_{n=1}^{N_2} C_{jn}^{(2)} w_{in} - \left(\mu^2 \sum_{m=1}^{N_1}\sum_{n=1}^{N_2} C_{im}^{(2)} C_{jn}^{(2)} w_{mn} + \mu^2\lambda^2 \sum_{n=1}^{N_2} C_{jn}^{(4)} w_{in}\right)\right]$$

$$+\bar{A}_{22}\left[\frac{\lambda}{\eta}\sum_{n=1}^{N_2}C_{jn}^{(1)}v_{in}+\frac{\lambda^2}{2\eta^2}\left(\sum_{n=1}^{N_2}C_{jn}^{(1)}w_{in}\right)^2\right]$$

$$\times\lambda^2\left[\sum_{n=1}^{N_2}C_{jn}^{(2)}w_{in}-\left(\mu^2\sum_{m=1}^{N_1}\sum_{n=1}^{N_2}C_{im}^{(2)}C_{jn}^{(2)}w_{mn}+\mu^2\lambda^2\sum_{n=1}^{N_2}C_{jn}^{(4)}w_{in}\right)\right],$$

$$\bar{Z}_2=\bar{A}_{66}\left(\frac{\lambda}{\eta}\sum_{m=1}^{N_1}\sum_{n=1}^{N_2}C_{im}^{(1)}C_{jn}^{(1)}u_{mn}+\frac{1}{\eta}\sum_{m=1}^{N_1}C_{im}^{(2)}v_{mj}\right)$$

$$\times\lambda\left[\sum_{n=1}^{N_2}C_{jn}^{(1)}w_{in}-\mu^2\left(\sum_{m=1}^{N_1}\sum_{n=1}^{N_2}C_{im}^{(2)}C_{jn}^{(1)}w_{mn}+\lambda^2\sum_{n=1}^{N_2}C_{jn}^{(3)}w_{in}\right)\right]$$

$$+\left(\frac{\lambda}{\eta^2}\sum_{n=1}^{N_2}C_{jn}^{(1)}w_{in}\times\sum_{m=1}^{N_1}C_{im}^{(2)}w_{mj}+\frac{\lambda}{\eta^2}\sum_{m=1}^{N_1}C_{im}^{(1)}w_{mj}\times\sum_{m=1}^{N_1}\sum_{n=1}^{N_2}C_{im}^{(1)}C_{jn}^{(1)}w_{mn}\right)$$

$$\times\lambda\left[\sum_{n=1}^{N_2}C_{jn}^{(1)}w_{in}-\mu^2\left(\sum_{m=1}^{N_1}\sum_{n=1}^{N_2}C_{im}^{(2)}C_{jn}^{(1)}w_{mn}+\lambda^2\sum_{n=1}^{N_2}C_{jn}^{(3)}w_{in}\right)\right]$$

$$+\bar{A}_{66}\left(\frac{\lambda^2}{\eta}\sum_{n=1}^{N_2}C_{jn}^{(2)}u_{in}+\frac{\lambda}{\eta}\sum_{m=1}^{N_1}\sum_{n=1}^{N_2}C_{im}^{(1)}C_{jn}^{(1)}v_{mn}\right)$$

$$\times\left[\sum_{m=1}^{N_1}C_{im}^{(1)}w_{mj}-\mu^2\left(\sum_{m=1}^{N_1}C_{im}^{(3)}w_{mj}+\lambda^2\sum_{m=1}^{N_1}\sum_{n=1}^{N_2}C_{im}^{(1)}C_{jn}^{(2)}w_{mn}\right)\right]$$

$$+\left(\frac{\lambda^2}{\eta^2}\sum_{n=1}^{N_2}C_{jn}^{(1)}w_{in}\times\sum_{m=1}^{N_1}\sum_{n=1}^{N_2}C_{im}^{(1)}C_{jn}^{(1)}w_{mn}+\frac{\lambda^2}{\eta^2}\sum_{m=1}^{N_1}C_{im}^{(1)}w_{mj}\times\sum_{n=1}^{N_2}C_{jn}^{(2)}w_{in}\right)$$

$$\times\left[\sum_{m=1}^{N_1}C_{im}^{(1)}w_{mj}-\mu^2\left(\sum_{m=1}^{N_1}C_{im}^{(3)}w_{mj}+\lambda^2\sum_{m=1}^{N_1}\sum_{n=1}^{N_2}C_{im}^{(1)}C_{jn}^{(2)}w_{mn}\right)\right]$$

$$+2\bar{A}_{66}\left(\frac{\lambda}{\eta}\sum_{n=1}^{N_2}C_{jn}^{(1)}u_{in}+\frac{1}{\eta}\sum_{m=1}^{N_1}C_{im}^{(1)}v_{mj}+\frac{\lambda}{\eta^2}\sum_{m=1}^{N_1}C_{im}^{(1)}w_{mj}\sum_{n=1}^{N_2}C_{jn}^{(1)}w_{in}\right)$$

$$\times\lambda\left[\sum_{m=1}^{N_1}\sum_{n=1}^{N_2}C_{im}^{(1)}C_{jn}^{(1)}w_{mn}-\mu^2\left(\sum_{m=1}^{N_1}\sum_{n=1}^{N_2}C_{im}^{(3)}C_{jn}^{(1)}w_{mn}+\lambda^2\sum_{m=1}^{N_1}\sum_{n=1}^{N_2}C_{im}^{(1)}C_{jn}^{(3)}\right)\right].\qquad\text{(C1)}$$

Appendix D

The discretized expressions for the boundary conditions in equations (28)-(30) are expressed as follows. For the SSSS boundary conditions, we have

$$w_{1j} = \varphi_{y,1j} = \phi_{1j} = 0,\ \sum_{m=1}^{N_1} C_{1m}^{(1)} \varphi_{x,mj} = 0,\ (\zeta = 0),$$

$$w_{N_1 j} = \varphi_{y,N_1 j} = \phi_{N_1 j} = 0,\ \sum_{m=1}^{N_1} C_{N_1 m}^{(1)} \varphi_{x,mj} = 0,\ (\zeta = 1),$$

$$w_{i1} = \varphi_{x,i1} = \phi_{i1} = 0,\ \sum_{n=1}^{N_2} C_{1n}^{(1)} \varphi_{y,in} = 0,\ (\xi = 0),$$

$$w_{iN_2} = \varphi_{x,iN_2} = \phi_{iN_2} = 0,\ \sum_{n=1}^{N_2} C_{N_2 n}^{(1)} \varphi_{y,in} = 0,\ (\xi = 1). \quad \text{(D1)}$$

For the CCCC boundary conditions, we have

$$w_{1j} = \varphi_{x,1j} = \varphi_{y,1j} = \phi_{1j} = 0,\ (\zeta = 0),$$

$$w_{N_1 j} = \varphi_{x,N_1 j} = \varphi_{y,N_1 j} = \phi_{N_1 j} = 0,\ (\zeta = 1),$$

$$w_{i1} = \varphi_{x,i1} = \varphi_{y,i1} = \phi_{i1} = 0,\ (\xi = 0),$$

$$w_{iN_2} = \varphi_{x,iN_2} = \varphi_{y,iN_2} = \phi_{iN_2} = 0,\ (\xi = 1). \quad \text{(D2)}$$

For the CCSS boundary conditions, we have

$$w_{1j} = \varphi_{x,1j} = \varphi_{y,1j} = \phi_{1j} = 0,\ (\zeta = 0),$$

$$w_{N_1 j} = \varphi_{y,N_1 j} = \phi_{N_1 j} = 0,\ \sum_{m=1}^{N_1} C_{N_1 m}^{(1)} \varphi_{x,mj} = 0,\ (\zeta = 1),$$

$$w_{i1} = \varphi_{x,i1} = \varphi_{y,i1} = \phi_{i1} = 0,\ (\xi = 0),$$

$$w_{iN_2} = \varphi_{x,iN_2} = \phi_{iN_2} = 0,\ \sum_{n=1}^{N_2} C_{N_2 n}^{(1)} \varphi_{y,in} = 0,\ (\xi = 1). \quad \text{(D3)}$$

Appendix E

The unknown displacement vectors $\{u_{ij}\}$, $\{v_{ij}\}$, $\{w_{ij}\}$, $\{\varphi_{x,ij}\}$, $\{\varphi_{y,ij}\}$, $\{\phi_{ij}\}$ in equation (35) are given as

$$\{u_{ij}\} = \{u_{11}, u_{12}, \cdots, u_{1N_2}, u_{21}, u_{22}, \cdots, u_{2N_2}, \cdots, u_{N_1 1}, u_{N_1 2}, \cdots, u_{N_1 N_2}\},$$

$$\{v_{ij}\} = \{v_{11}, v_{12}, \cdots, v_{1N_2}, v_{21}, v_{22}, \cdots, v_{2N_2}, \cdots, v_{N_1 1}, v_{N_1 2}, \cdots, v_{N_1 N_2}\},$$

$$\{w_{ij}\} = \{w_{11}, w_{12}, \cdots, w_{1N_2}, w_{21}, w_{22}, \cdots, w_{2N_2}, \cdots, w_{N_1 1}, w_{N_1 2}, \cdots, w_{N_1 N_2}\},$$

$$\left\{\varphi_{x,ij}\right\}=\left\{\varphi_{x,11},\varphi_{x,12},\cdots,\varphi_{x,1N_2},\varphi_{x,21},\varphi_{x,22},\cdots,\varphi_{x,2N_2},\cdots,\varphi_{x,N_11},\varphi_{x,N_12},\cdots,\varphi_{x,N_1N_2}\right\},$$

$$\left\{\varphi_{y,ij}\right\}=\left\{\varphi_{y,11},\varphi_{y,12},\cdots,\varphi_{y,1N_2},\varphi_{y,21},\varphi_{y,22},\cdots,\varphi_{y,2N_2},\cdots,\varphi_{y,N_11},\varphi_{y,N_12},\cdots,\varphi_{y,N_1N_2}\right\},$$

$$\left\{\phi_{ij}\right\}=\left\{\phi_{11},\phi_{12},\cdots,\phi_{1N_2},\phi_{21},\phi_{22},\cdots,\phi_{2N_2},\cdots,\phi_{N_11},\phi_{N_12},\cdots,\phi_{N_1N_2}\right\}. \quad \text{(E1)}$$

References

1. K. S. Novoselov, A. K. Geim, S. V. Morozov, D. Jiang, Y. Zhang, S. V. Dubonos, I. V. Grigorieva and A. A. Firsov, Electric field effect in atomically thin carbon films, Science 306, p666-669, 2004.
2. A. A. Balandin, S. Ghosh, W. Bao, I. Calizo, D. Teweldebrhan, F. Miao and C. N. Lau, Superior thermal conductivity of single-layer graphene, Nano Letters 8, p902-907, 2008.
3. A. Lee, X. Wei, J. W. Kysar and J. Hone, Measurement of the elastic properties and intrinsic strength of monolayer graphene, Science 321, p385-388, 2008.
4. M. A. Rafiee, J. Rafiee, Z. Wang, H. Song, Z. Z. Yu and N. Koratkar, Enhanced mechanical properties of nanocomposites at low graphene content, ACS nano 3, p3884-3890, 2009.
5. R. K. Layek, S. Samanta, D. P. Chatterjee and A. K. Nandi, Physical and mechanical properties of poly(methyl methacrylate)-functionalized graphene/poly(vinylidine fluoride) nanocomposites piezoelectric beta polymorph formation, Polymer 51, p5846-5856, 2010.
6. W. Lu, J. X. Weng, D. J. Wu, C. L. Wu and G. H. Chen, Epoxy resin/graphite electrically conductive nanosheet nanocomposite, Materials and Manufacturing Processes 21, p167-171, 2006.
7. J. J. Mao, L. L. Ke, J. Yang, S. Kitipornchai and Y. S. Wang, Thermoelastic instability of functionally graded materials with interaction of frictional heat and contact resistance, Mechanics Based Design of Structures and Machines 46, p136-156, 2018.
8. Y. X. Hao, L. H. Chen, W. Zhang and J. G. Lei, Nonlinear oscillations, bifurcations and chaos of functionally graded materials plate, Journal of Sound and Vibration 312, p862-892, 2008.
9. S. Suresh and A. Mortensen, Fundamentals of functionally graded materials, The Institut of Materials, 1998.

10. W. Zhang, J. Yang and Y. X. Hao, Chaotic vibrations of an orthotropic FGM rectangular plate based on third-order shear deformation theory, Nonlinear Dynamics 59, p619-660, 2010.
11. Y. X. Hao, W. Zhang and J. Yang, Nonlinear oscillations of a cantilever FGM rectangular plate based on third-order plate theory and asymptotic perturbation method, Composites Part B: Engineering 42, p402-413, 2011.
12. W. Zhang, Y. X. Hao, X. Y. Guo and L. H. Chen, Complicated nonlinear responses of a simply supported FGM rectangular plate under combined parametric and external excitations, Meccanica 47, p 985-1014, 2012.
13. Y. X. Hao, W. Zhang, J. Yang, Nonlinear dynamics of a FGM plate with two clamped opposite edges and two free edges, Acta Mechanica Solida Sinica 27, p394-406, 2014.
14. W. Zhang, Y. X. Hao and J. Yang, Nonlinear dynamics of FGM circular cylindrical shell with clamped-clamped edges, Composite Structures 94, p1075-1086, 2012.
15. C. Feng, S. Kitipornchai and J. Yang, Nonlinear free vibration of functionally graded polymer composite beams reinforced with graphene nanoplatelets (GNPLs), Engineering Structures 140, p110-119, 2017.
16. M. T. Song, S. Kitipornchai and J. Yang, Free and forced vibrations of functionally graded polymer composite plates reinforced with graphene nanoplatelets, Composite Structures 159, p579-588, 2017.
17. B. Yang, J. Mei, D. Chen, F. Yu and J. Yang, 3D thermo-mechanical solution of transversely isotropic and functionally graded graphene reinforced elliptical plates, Composite Structures 184, p1040-1048, 2018.
18. H. S. Shen, Y. Xiang and Y. Fan, Nonlinear vibration of thermally postbuckled FG-GRC laminated beams resting on elastic foundations, International Journal of Structural Stability and Dynamics p1950051, 2019.
19. H. S. Shen, Y. Xian, Y. Fan and D. Hui, Nonlinear vibration of functionally graded graphene-reinforced composite laminated cylindrical panels resting on elastic foundations in thermal environments, Composites Part B-Engineering 136, p177-186, 2018.
20. H. S. Shen, Y. Xiang and F. Lin, Nonlinear vibration of functionally graded graphene-reinforced composite laminated plates in thermal environments, Computer Methods in Applied Mechanics and Engineering 319, p175-193, 2017.
21. Y. Kiani, Isogeometric large amplitude free vibration of graphene reinforced laminated plates in thermal environment using nurbs formulation, Computer Methods in Applied

Mechanics and Engineering 332, p86-101, 2018.
22. S. J. Zhang, R. Xia, L. Lebrun, D. Anderson and T. R. Shrout, Piezoelectric materials for high power, high temperature applications, Materials Letters 59, p3471-3475, 2005.
23. A. Witvrouw and A. Mehta, The use of functionally graded poly-sige layers for mems applications, Functionally Graded Materials Viii 492-493, p255-260, 2005.
24. Z. G. Song, L. W. Zhang and K. M. Liew, Active vibration control of CNT-reinforced composite cylindrical shells via piezoelectric patches, Composite Structures 158, p92-100, 2016.
25. W. Zhang, Z. G. Yao and M. H. Yao, Periodic and chaotic dynamics of composite laminated piezoelectric rectangular plate with one-to-two internal resonance, Science in China Series E: Technological Sciences 52, p731-742, 2009.
26. W. Zhang and W. L. Hao, Multi-pulse chaotic dynamics of six-dimensional non-autonomous nonlinear system for a composite laminated piezoelectric rectangular plate, Nonlinear Dynamics 73, p1005-1033, 2013.
27. M. H. Yao and W. Zhang, Multi-pulse chaotic motions of high-dimension nonlinear system for a laminated composite piezoelectric rectangular plate, Meccanica 49, p365-392, 2014.
28. M. H. Yao, W. Zhang and Z. G. Yao, Nonlinear vibrations and chaotic dynamics of the laminated composite piezoelectric beam, Journal of Vibration and Acoustics 137, p011002, 2015.
29. B. A. Selim, L. W. Zhang and K. M. Liew, Active vibration control of CNT-reinforced composite plates with piezoelectric layers based on reddy's higher-order shear deformation theory, Composite Structures 163, p350-364, 2017.
30. L. W. Zhang, Z. G. Song and K. M. Liew, Modeling aerothermoelastic properties and active flutter control of nanocomposite cylindrical shells in supersonic airflow under thermal environments, Computer Methods in Applied Mechanics and Engineering 325, p416-433, 2017.
31. Y. F. Zhang, W. Zhang and Z. G. Yao, Analysis on nonlinear vibrations near internal resonances of a composite laminated piezoelectric rectangular plate, Engineering Structures 173, p89-106, 2018.
32. S. F. Lu, W. Zhang and X. J. Song, Time-varying nonlinear dynamics of a deploying piezoelectric laminated composite plate under aerodynamic force, Acta Mechanica Sinica 34, p303-314, 2018.
33. N. Maity, A. Mandal and A. K. Nandi, Hierarchical nanostructured polyaniline

functionalized graphene/poly (vinylidene fluoride) composites for improved dielectric performances, Polymer 103, p83-97, 2016.

34. M. Abbasipour, R. Khajavi, A. A. Yousefi, M. E. Yazdanshenas and F. Razaghian, The piezoelectric response of electrospun PVDF nanofibers with graphene oxide, graphene, and halloysite nanofillers: A comparative study, Journal of Materials Science-Materials in Electronics 28, p15942-15952, 2017.
35. J. J. Mao and W. Zhang, Linear and nonlinear free and forced vibrations of graphene reinforced piezoelectric composite plate under external voltage excitation, Composite Structures 203, p551-565, 2018.
36. J. J. Mao and W. Zhang, Buckling and post-buckling analyses of functionally graded graphene reinforced piezoelectric plate subjected to electric potential and axial forces, Composite Structures 216, p392-405, 2019.
37. X. Y. Guo, P. Jiang, W. Zhang, J. Yang, S. Kitipornchai and L. Sun, Nonlinear dynamic analysis of composite piezoelectric plates with graphene skin, Composite Structures 206, p839-852, 2018.
38. K. Xu, K. Wang, W. Zhao, W. Z. Bao, E. Liu, Y. F. Ren, M. Wang, Y. J. Fu, J. W. Zeng, Z. G. Li, W. Zhou, F. Q. Song, X. R. Wang, Y. Shi, X. G. Wan, M. S. Fuhrer, B. G. Wang, Z. H. Qiao, F. Miao and D. Y. Xing, The positive piezoconductive effect in graphene, Nature Communications 6, 2015.
39. M. M. Abolhasani, K. Shirvanimoghaddam and M. Naebe, PVDF/graphene composite nanofibers with enhanced piezoelectric performance for development of robust nanogenerators, Composites Science and Technology 138, p49-56, 2017.
40. T. K. Das and S. Prusty, Graphene-based polymer composites and their applications, Polymer-Plastics Technology and Engineering 52, p319-331, 2013.
41. J. S. Stolken and A. G. Evans, A microbend test method for measuring the plasticity length scale, Acta Materialia 46, p5109-5115, 1998.
42. W. D. Nix, Mechanical-properties of thin-films, Metallurgical Transactions a-Physical Metallurgy and Materials Science 20, p2217-2245, 1989.
43. N. A. Fleck, G. M. Muller, M. F. Ashby and J. W. Hutchinson, Strain gradient plasticity-theory and experiment, Acta Metallurgica Et Materialia 42, p475-487, 1994.
44. A. C. M. Chong and D. C. C. Lam, Strain gradient plasticity effect in indentation hardness of polymers, Journal of Materials Research 14, p4103-4110, 1999.
45. R. Mindlin and H. Tiersten, Effects of couple-stresses in linear elasticity, Archive for Rational Mechanics and Analysis 11, p415-448, 1962.

46. B. L. Wang, M. C. Liu, J. F. Zhao and S. J. Zhou, A size-dependent Reddy–Levinson beam model based on a strain gradient elasticity theory, Meccanica 49, p1427-1441, 2014.
47. M. C. Liu, J. Wu, Y. X. Gan and C. Q. Chen, The pore-load modulus of ordered nanoporous materials with surface effects, AIP Advances 6, p035324, 2016.
48. A. C. Eringen, Nonlocal continuum field theories, Springer Science & Business Media, 2002.
49. J. N. Reddy, Nonlocal nonlinear formulations for bending of classical and shear deformation theories of beams and plates, International Journal of Engineering Science 48, p1507-1518, 2010.
50. L. L. Ke, C. Liu and Y. S. Wang, Free vibration of nonlocal piezoelectric nanoplates under various boundary conditions, Physica E: Low-Dimensional Systems and Nanostructures 66, p93-106, 2015.
51. C. Liu, L. L. Ke, J. Yang, S. Kitipornchai and Y. S. Wang, Nonlinear vibration of piezoelectric nanoplates using nonlocal mindlin plate theory, Mechanics of Advanced Materials and Structures 25, p1252-1264, 2018.
52. Y. Zhang, Z. X. Lei, L. W. Zhang, K. M. Liew and J. L. Yu, Nonlocal continuum model for vibration of single-layered graphene sheets based on the element-free kp-Ritz method, Engineering Analysis with Boundary Elements 56, p90-97, 2015.
53. Y. Zhang, L. W. Zhang, K. M. Liew and J. L. Yu, Nonlocal continuum model for large deformation analysis of SLGSs using the kp-Ritz element-free method, International Journal of Non-Linear Mechanics 79, p1-9, 2016.
54. Y. Zhang, L. W. Zhang, K. M. Liew and J. L. Yu, Buckling analysis of graphene sheets embedded in an elastic medium based on the kp-Ritz method and non-local elasticity theory, Engineering Analysis with Boundary Elements 70, p31-39, 2016.
55. S. Sahmani, M. M. Aghdam and T. Rabczuk, Nonlinear bending of functionally graded porous micro/nano-beams reinforced with graphene platelets based upon nonlocal strain gradient theory, Composite Structures 186, p68-78, 2018.
56. S. Sahmani and M. Aghdam, Nonlinear instability of axially loaded functionally graded multilayer graphene platelet-reinforced nanoshells based on nonlocal strain gradient elasticity theory, International Journal of Mechanical Sciences 131, p95-106, 2017.
57. A. Nieto, A. Bisht, D. Lahiri, C. Zhang and A. Agarwal, Graphene reinforced metal and ceramic matrix composites: A review, International Materials Reviews 62, p241-302, 2017.

58. S. T. Quek and Q. Wang, On dispersion relations in piezoelectric coupled-plate structures, Smart Materials and Structures 9, p859, 2000.
59. Q. Wang, On buckling of column structures with a pair of piezoelectric layers, Engineering Structures 24, p199-205, 2002.
60. R. Bellman, B. G. Kashef and J. Casti, Differential quadrature: a technique for the rapid solution of nonlinear partial differential equations, Journal of Computational Physics 10, p40-52, 1972.
61. J. R. Quan and C. T. Chang, New insights in solving distributed system equations by the quadrature method-I. analysis, Computers and Chemical Engineering 13, p779-788, 1989.
62. C. Shu, Differential quadrature and its application in engineering, Springer Science and Business Media, 2012.
63. C. W. Bert and M. Malik, Differential quadrature: a powerful new technique for analysis of composite structures, Composite structures 39, p179-189, 1997.
64. W. Zhang, D. M. Wang and M. H. Yao, Using Fourier differential quadrature method to analyze transverse nonlinear vibrations of an axially accelerating viscoelastic beam, Nonlinear Dynamics 78, p839-856, 2014.
65. H. Ersoy, K. Mercan and Ö. Civalek, Frequencies of FGM shells and annular plates by the methods of discrete singular convolution and differential quadrature methods, Composite Structures, 183, 7-20, 2018.
66. H. C. Li, L. L. Ke, J. Yang, S. Kitipornchai and Y. S. Wang, Free vibration of variable thickness FGM beam submerged in fluid, Composite Structures, 111582, 2019.

Table Captions

Table 1 Piezoelectric properties of the PVDF are shown.

Table 2 The convergence of the discretization in the DQ method N_0 is indicated.

Table 3 The dimensionless linear frequencies are obtained for a nonlocal piezoelectric microplate with the SSSS boundary conditions, different geometrical parameter and different nonlocal parameter n.

Table 4 The effect of the nonlocal parameter on the nonlinear frequency ratio ω_{nl} / ω_l is given for a PZT-4 microplate.

Table 5 The dimensionless nonlinear frequencies are given for a macroscopic GNPL reinforced functionally gradient piezoelectric plate with the CCCC boundary conditions and different GNPL volume fractions.

Table 1

$e_{31,M}$ $\left(C/m^2\right)$	$e_{32,M}$ $\left(C/m^2\right)$	$e_{24,M}$ $\left(C/m^2\right)$	$e_{15,M}$ $\left(C/m^2\right)$	$\kappa_{11,M}$ $\left(C/Vm\right)$	$\kappa_{22,M}$ $\left(C/Vm\right)$	$\kappa_{33,M}$ $\left(C/Vm\right)$
50.54 $\times 10^{-3}$	13.21 $\times 10^{-3}$	-12.65 $\times 10^{-3}$	-15.93 $\times 10^{-3}$	0.5385 $\times 10^{-9}$	0.6638 $\times 10^{-9}$	0.5957 $\times 10^{-9}$

Table 2

N_0	$w_{\max}/h_M = 0.2$	$w_{\max}/h_M = 0.4$	$w_{\max}/h_M = 0.6$
	ω_{nl}/ω_l	ω_{nl}/ω_l	ω_{nl}/ω_l
5	0.9976	0.9903	0.9779
7	1.0081	1.0316	1.0677
9	1.0069	1.0268	1.0575
11	1.0074	1.0287	1.0615
13	1.0073	1.0283	1.0608
15	1.0073	1.0284	1.0611
17	1.0073	1.0284	1.0611

Table 3

ω_l	$a_M = 10h_M$		$a_M = 40h_M$	
	Ke et al. [50]	Present	Ke et al. [50]	Present
$\mu = 0$	0.6068	0.6068	0.1570	0.1570
$\mu = 0.1$	0.5545	0.5545	0.1435	0.1435
$\mu = 0.2$	0.4536	0.4536	0.1174	0.1174
$\mu = 0.3$	0.3641	0.3641	0.0943	0.0943
$\mu = 0.4$	0.2976	0.2976	0.0770	0.0770
$\mu = 0.5$	0.2491	0.2491	0.0645	0.0645

Table 4

μ	$w_{\max}/h_M = 0.3$		$w_{\max}/h_M = 0.6$		$w_{\max}/h_M = 0.9$	
	Liu et al. [51]	Present	Liu et al. [51]	Present	Liu et al. [51]	Present
0	1.0536	1.0536	1.1930	1.1930	1.3813	1.3813
0.05	1.0550	1.0550	1.1967	1.1967	1.3860	1.3860
0.10	1.0590	1.0590	1.2069	1.2069	1.3977	1.3977
0.15	1.0654	1.0654	1.2226	1.2226	1.4145	1.4145

Table 5

ω_{nl}	$V_{gpl} = 0.25\%$		$V_{gpl} = 0.50\%$		$V_{gpl} = 0.75\%$	
	Mao et al. [35]	Present	Mao et al. [35]	Present	Mao et al. [35]	Present
U	1.4290	1.4293	1.7623	1.7628	2.0432	2.0437
X	1.5328	1.5331	1.9279	1.9284	2.2564	2.2568
O	1.3093	1.3096	1.5624	1.5629	1.7803	1.7809

Figure Captions

Figure 1 A GNPL reinforced functionally graded piezoelectric composite microplate subjected to an external electric potential resting on the Winkler elastic foundation is shown.

Figure 2 The GNPL distribution patterns along the thickness direction are demonstrated, (a) U pattern, (b) X pattern, (c) O pattern.

Figure 3 The effects of the total number *N* are shown on (a) the dimensionless linear vibration frequency, (b) the dimensionless nonlinear vibration frequency of the GNPL reinforced functionally gradient piezoelectric composite microplate under different boundary conditions and different GNPL distribution patterns.

Figure 4 The effect of the GNPLs piezoelectric multiple on the dimensionless linear vibration frequency is shown for the GNPL reinforced functionally gradient piezoelectric composite microplate under different boundary conditions and different GNPL distribution patterns.

Figure 5 The effect of the nonlocal coefficients on the dimensionless linear frequency is shown for the GNPL reinforced functionally gradient piezoelectric composite microplate.

Figure 6 The effect of the elastic coefficient of the Winkler elastic foundation on the dimensionless linear frequency is given for the GNPL reinforced functionally gradient piezoelectric composite microplate with different nonlocal coefficients.

Figure 7 The effect of the elastic coefficient of the Winkler elastic foundation on the dimensionless linear frequency is obtained for the GNPL reinforced functionally gradient piezoelectric composite microplate with different GNPL volume fractions.

Figure 8 The effect of the length-to-thickness ratio of the GNPL nanofillers on the dimensionless linear frequency is demonstrated for the GNPL reinforced functionally gradient piezoelectric composite microplate with different nonlocal coefficients.

Figure 9 The effect of the length-to-thickness ratio of the GNPL nanofillers on the dimensionless linear frequency is given for the GNPL reinforced functionally gradient piezoelectric composite microplate with different GNPL volume fractions.

Figure 10 The effect of the external voltage on the dimensionless linear frequency is illustrated for the GNPL reinforced functionally gradient piezoelectric composite microplate with varying GNPLs piezoelectric multiple.

Figure 11 The effect of the external voltage on the nonlinear frequency ratio is shown for the GNPL reinforced functionally gradient piezoelectric composite microplates with varying GNPL piezoelectric multiples.

Figure 12 The effect of the GNPLs piezoelectric multiple on the nonlinear frequency ratio is given for the GNPL reinforced functionally gradient piezoelectric composite microplate with the vibration amplitude $w_{\max}/h$ = 0.4 and different nonlocal coefficients.

Figure 13 The effect of the nonlocal coefficients on the nonlinear frequency ratio is obtained for the GNPL reinforced functionally gradient piezoelectric composite microplate.

Figure 14 The effect of the GNPL volume fractions on the nonlinear frequency ratio is illustrated for the GNPL reinforced functionally gradient piezoelectric composite microplate.

Figure 15 The effect of the elastic coefficient of the Winkler elastic foundation on the nonlinear frequency ratio is shown for the GNPL reinforced functionally gradient piezoelectric composite microplate.

Figure 16 The effect of the GNPL length-to-thickness ratio on the nonlinear frequency ratio is given for the GNPL reinforced functionally gradient piezoelectric composite microplate.

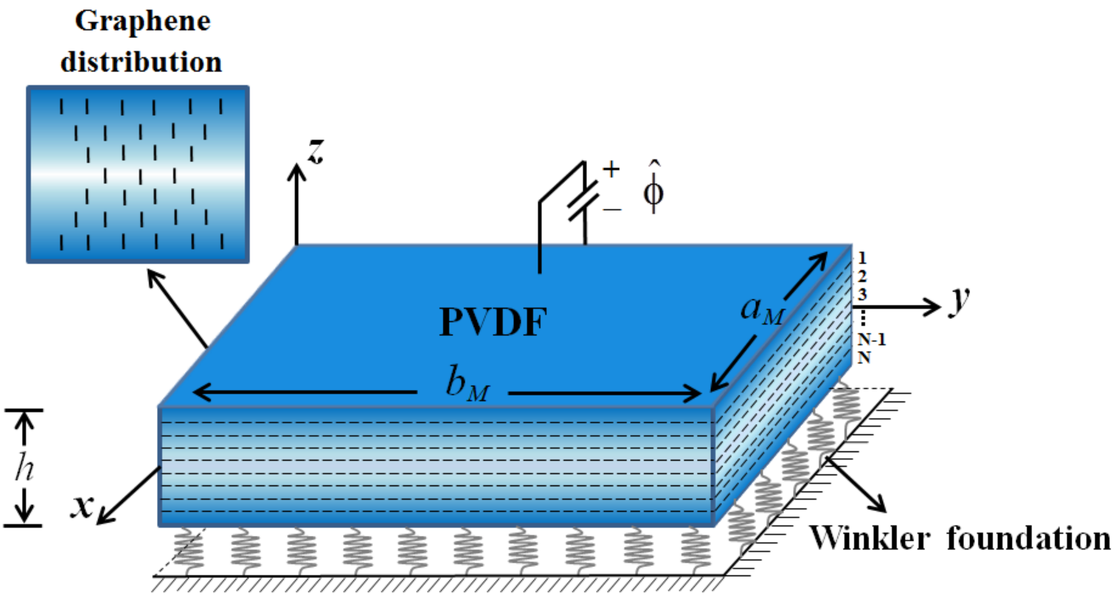
Graphene
distribution
z
+
–
$\hat{\phi}$
1
2
3
N-1
N
y
PVDF
a_M
b_M
h
x
Winkler foundation

Figure 1

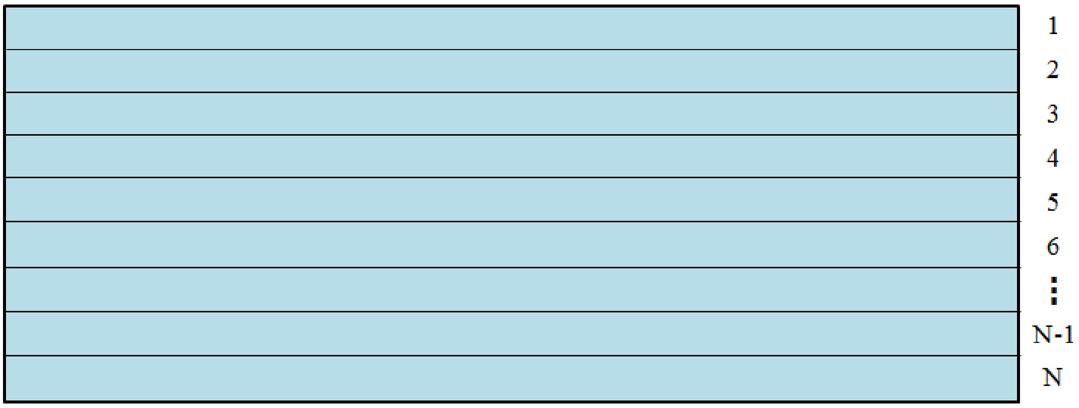

(a)

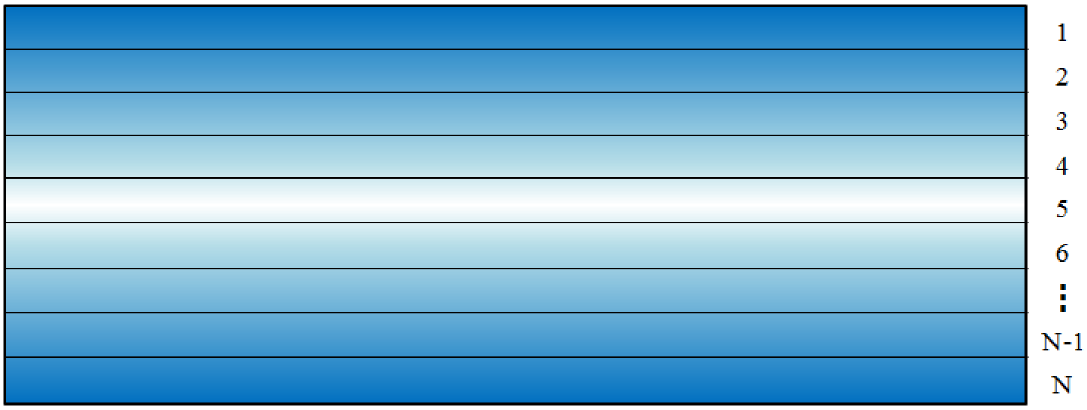

(b)

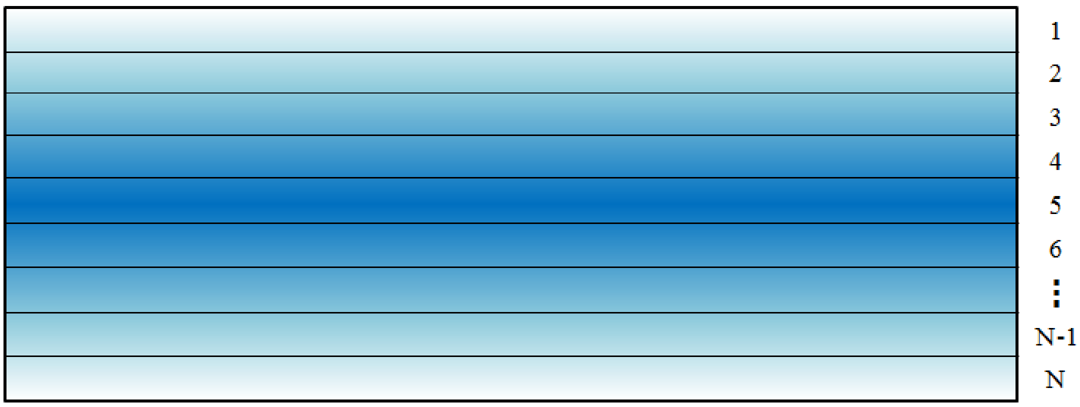

(c)

Figure 2

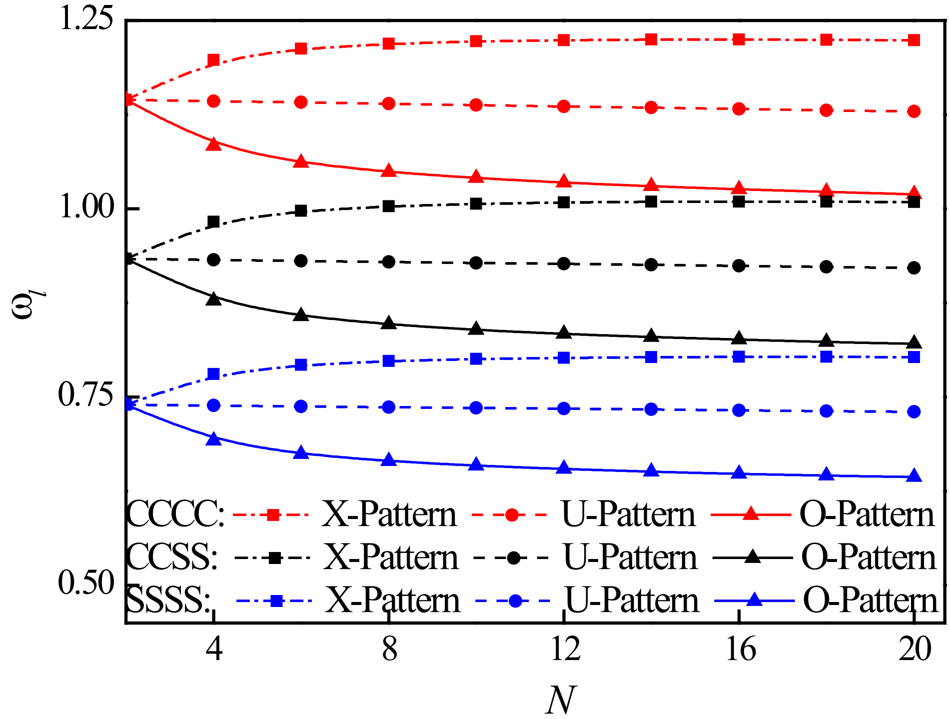
1.25
1.00
0.75
0.50
ω_l
4
8
12
16
20
N
CCCC: X-Pattern U-Pattern O-Pattern
CCSS: X-Pattern U-Pattern O-Pattern
SSSS: X-Pattern U-Pattern O-Pattern

(a)

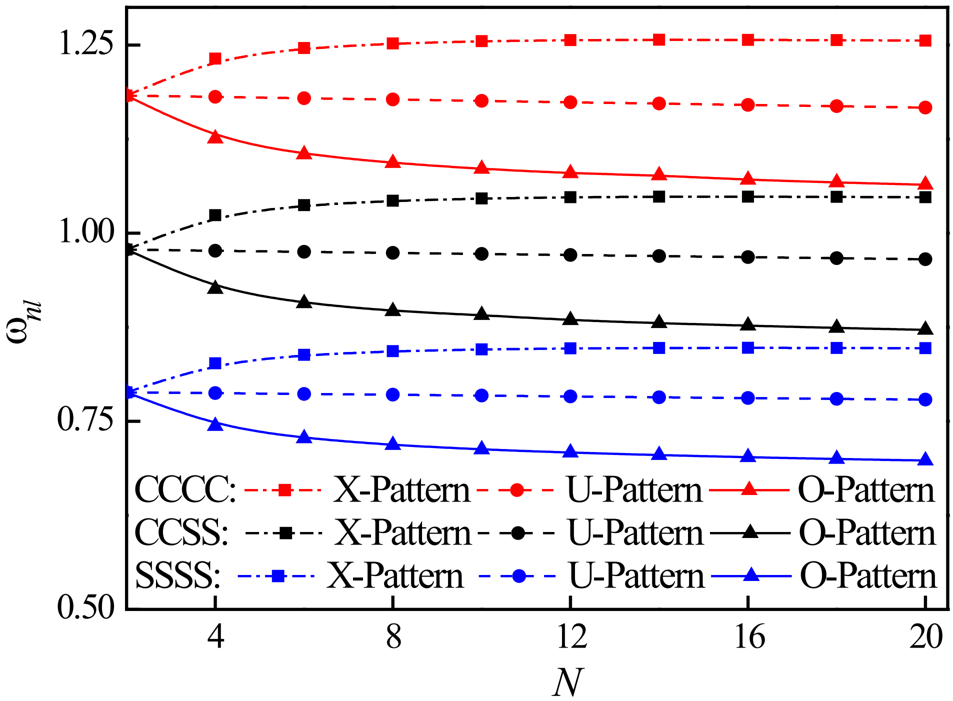
1.25
1.00
0.75
0.50
ω_{nl}
4
8
12
16
20
N
CCCC: X-Pattern U-Pattern O-Pattern
CCSS: X-Pattern U-Pattern O-Pattern
SSSS: X-Pattern U-Pattern O-Pattern

(b)

Figure 3

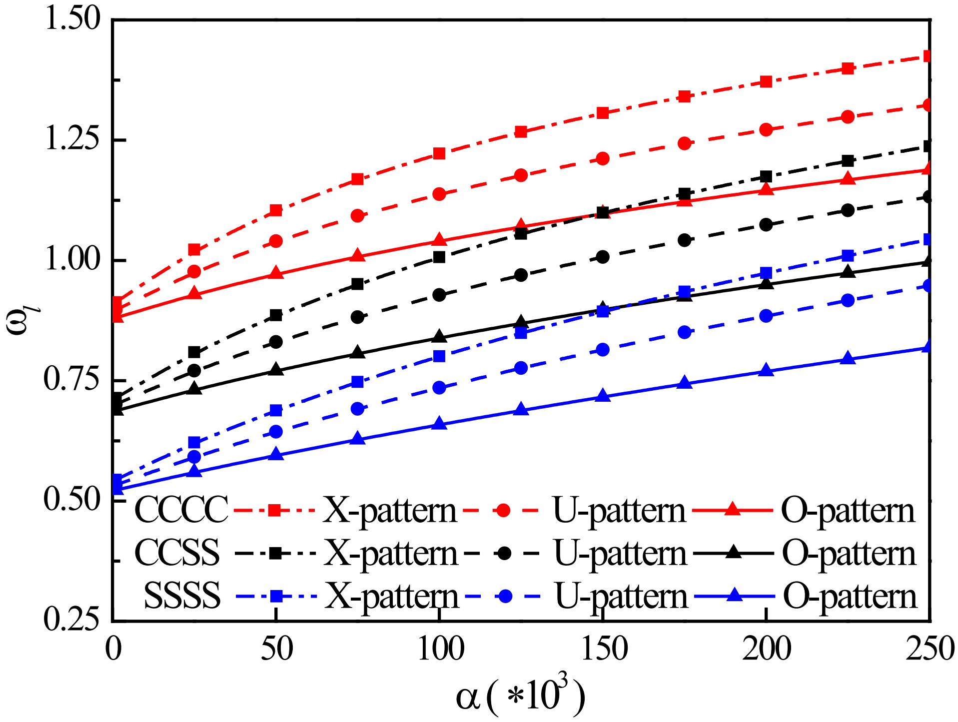

1.50
1.25
1.00
0.75
0.50
0.25
ω_l
CCCC X-pattern U-pattern O-pattern
CCSS X-pattern U-pattern O-pattern
SSSS X-pattern U-pattern O-pattern
0
50
100
150
200
250
$\alpha\,(*10^3)$

Figure 4

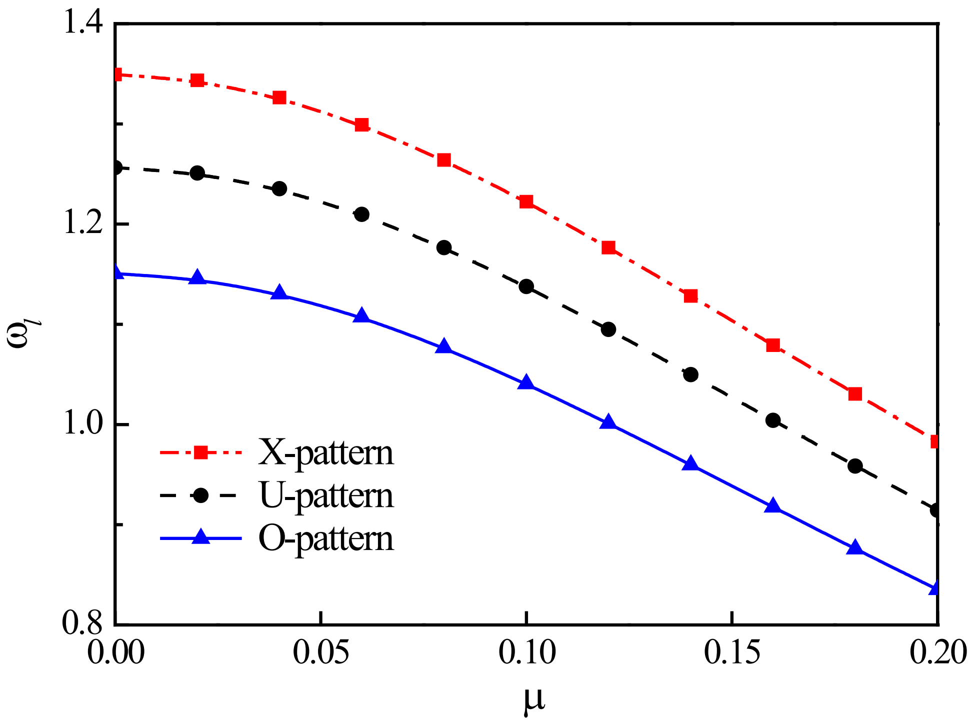
1.4
1.2
1.0
0.8
ω_l
0.00
0.05
0.10
0.15
0.20
μ
X-pattern
U-pattern
O-pattern

Figure 5

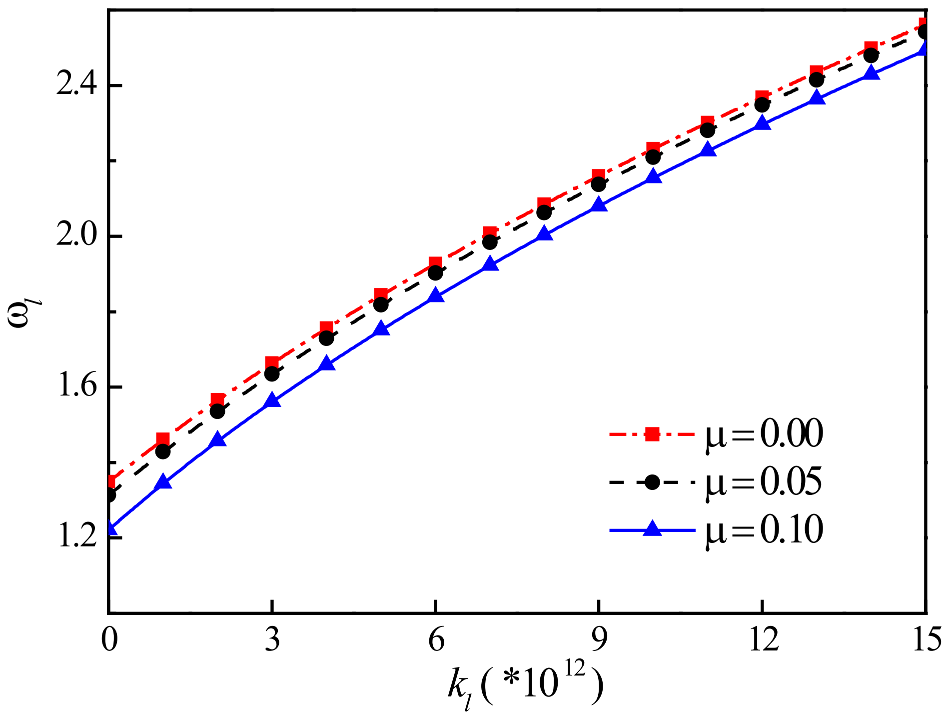

Figure 6

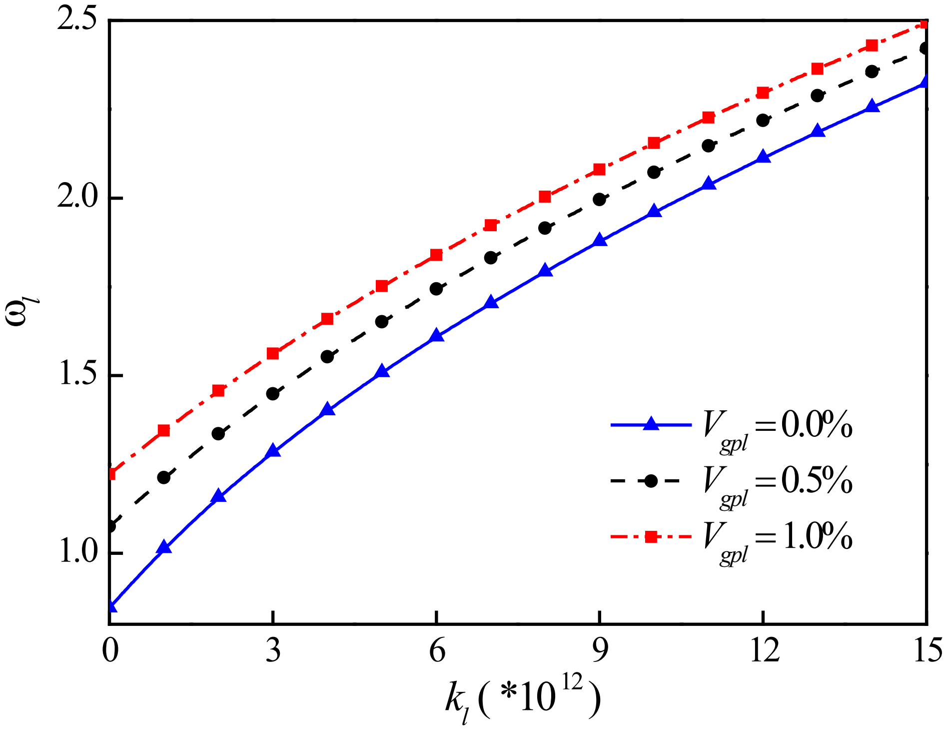

Figure 7

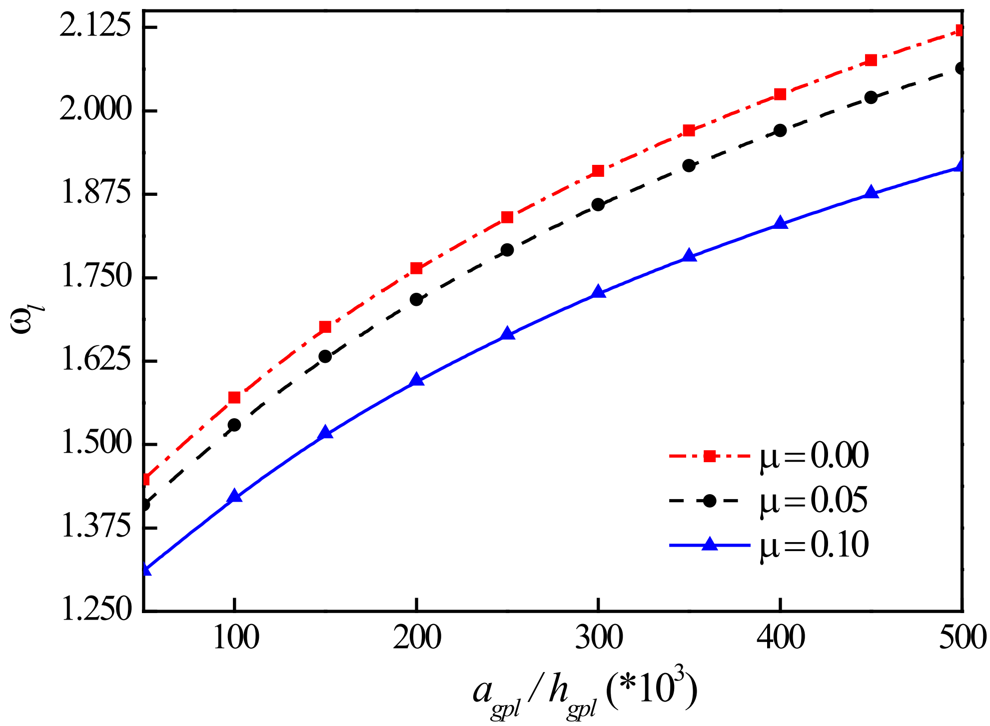
2.125
2.000
1.875
1.750
1.625
1.500
1.375
1.250
ω_l
100
200
300
400
500
a_{gpl}/h_{gpl} (*10^3)
μ=0.00
μ=0.05
μ=0.10

Figure 8

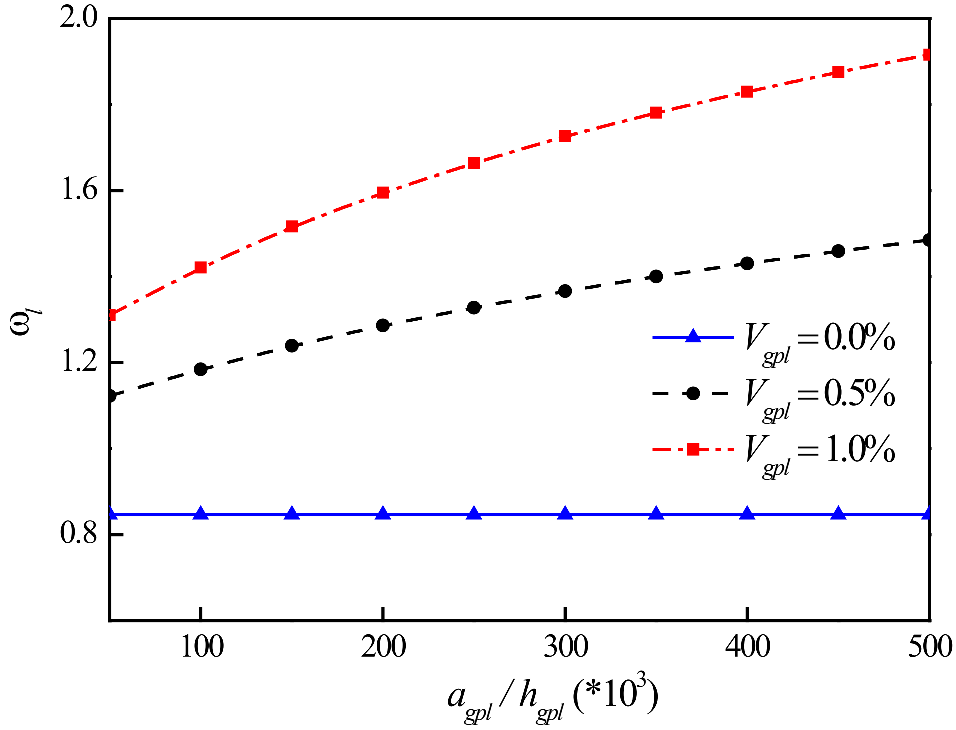

2.0
1.6
1.2
0.8
ω_l
$V_{gpl} = 0.0\%$
$V_{gpl} = 0.5\%$
$V_{gpl} = 1.0\%$
100
200
300
400
500
a_{gpl} / h_{gpl} (*10^3)

Figure 9

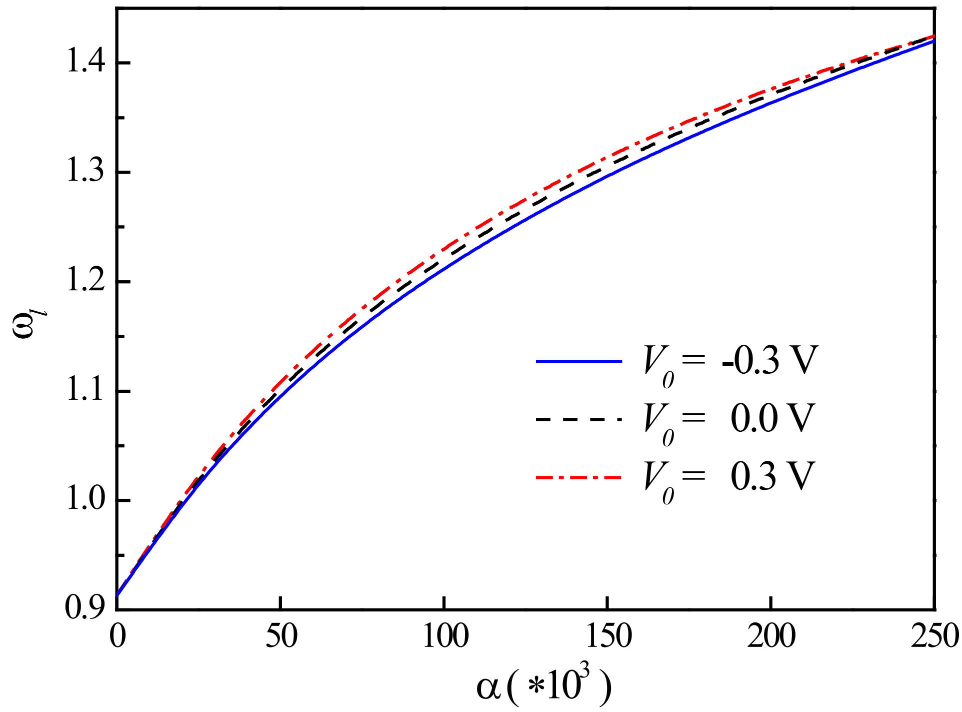

1.4
1.3
1.2
1.1
1.0
0.9
ω_l
0
50
100
150
200
250
$\alpha(*10^3)$
V_0 = -0.3 V
V_0 = 0.0 V
V_0 = 0.3 V

Figure 10

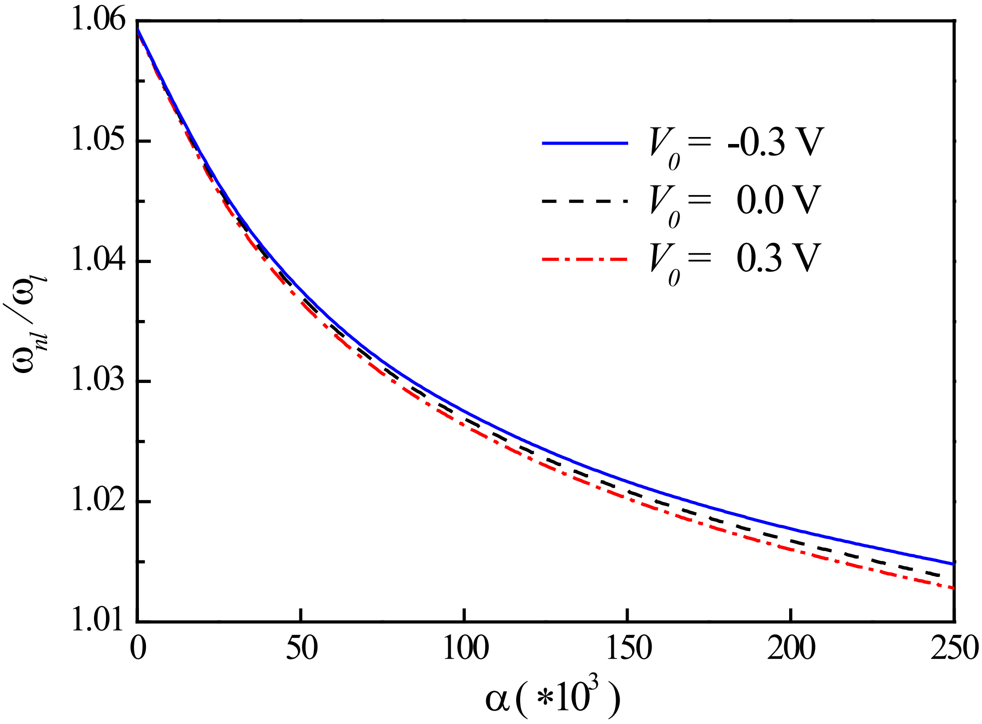
1.06
1.05
1.04
1.03
1.02
1.01
0
50
100
150
200
250
ω_{nl}/ω_l
$\alpha(*10^3)$
V_0 = -0.3 V
V_0 = 0.0 V
V_0 = 0.3 V

Figure 11

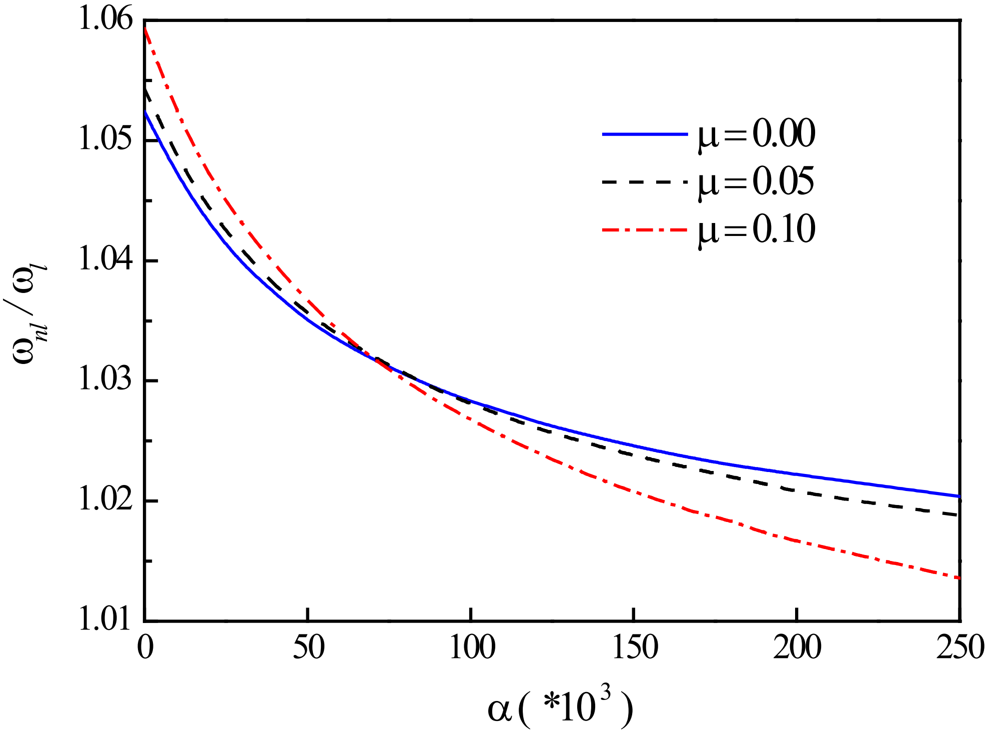
1.06
1.05
1.04
1.03
1.02
1.01
ω_nl / ω_l
0
50
100
150
200
250
α(*10³)
μ=0.00
μ=0.05
μ=0.10

Figure 12

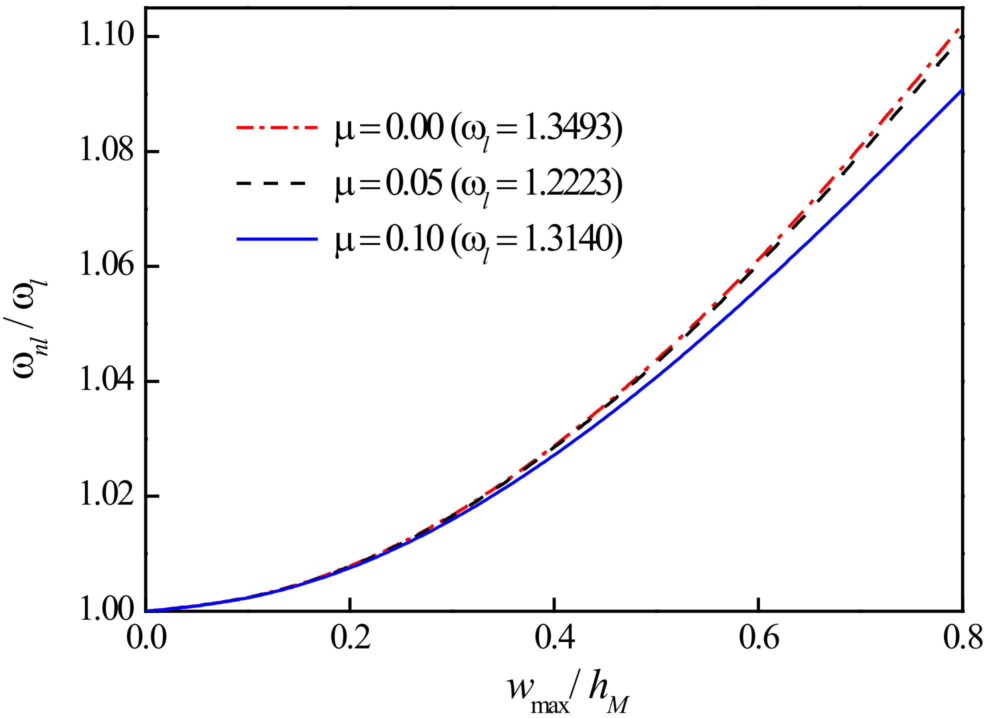
1.10
1.08
1.06
1.04
1.02
1.00
0.0
0.2
0.4
0.6
0.8
ω_{nl} / ω_l
$w_{\max} / h_M$
$\mu = 0.00$ ($\omega_l = 1.3493$)
$\mu = 0.05$ ($\omega_l = 1.2223$)
$\mu = 0.10$ ($\omega_l = 1.3140$)

Figure 13

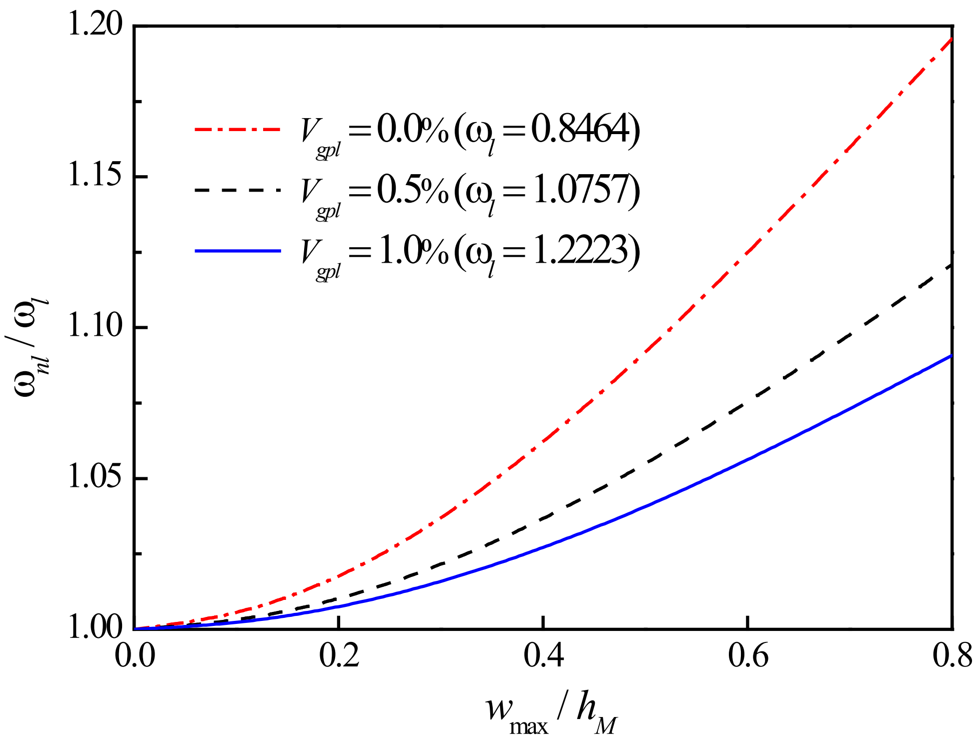

$V_{gpl} = 0.0\%\ (\omega_l = 0.8464)$
$V_{gpl} = 0.5\%\ (\omega_l = 1.0757)$
$V_{gpl} = 1.0\%\ (\omega_l = 1.2223)$
1.20
1.15
1.10
1.05
1.00
ω_{nl} / ω_l
0.0
0.2
0.4
0.6
0.8
$w_{\max} / h_M$

Figure 14

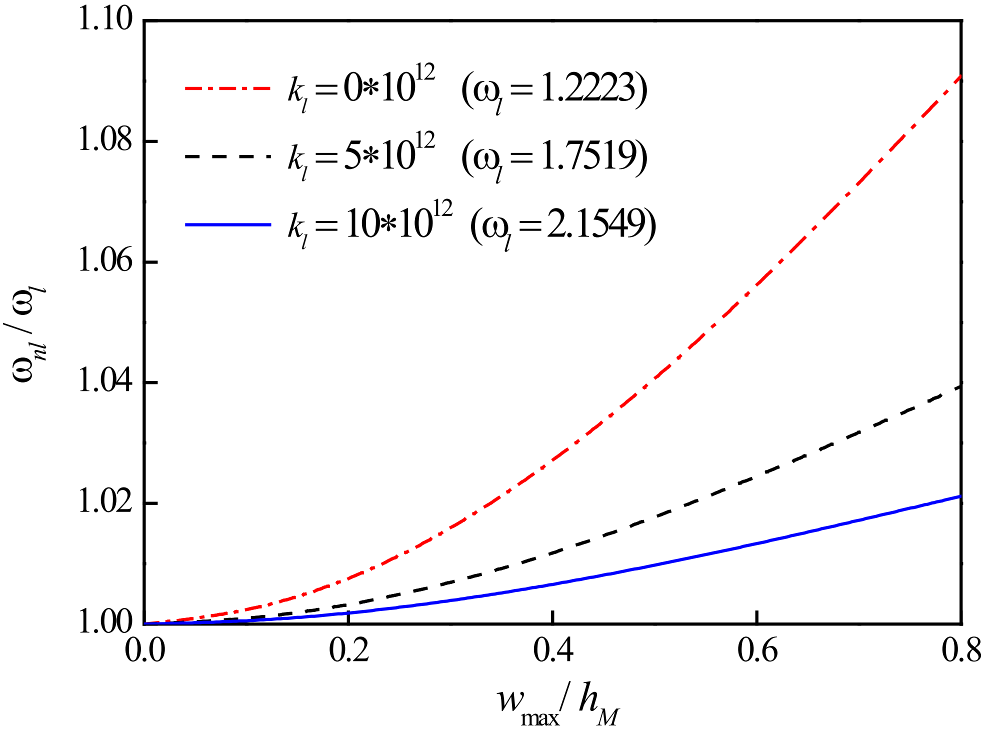
$k_l = 0*10^{12}$ ($\omega_l = 1.2223$)
$k_l = 5*10^{12}$ ($\omega_l = 1.7519$)
$k_l = 10*10^{12}$ ($\omega_l = 2.1549$)
ω_{nl} / ω_l
$w_{\max} / h_M$
1.00
1.02
1.04
1.06
1.08
1.10
0.0
0.2
0.4
0.6
0.8

Figure 15

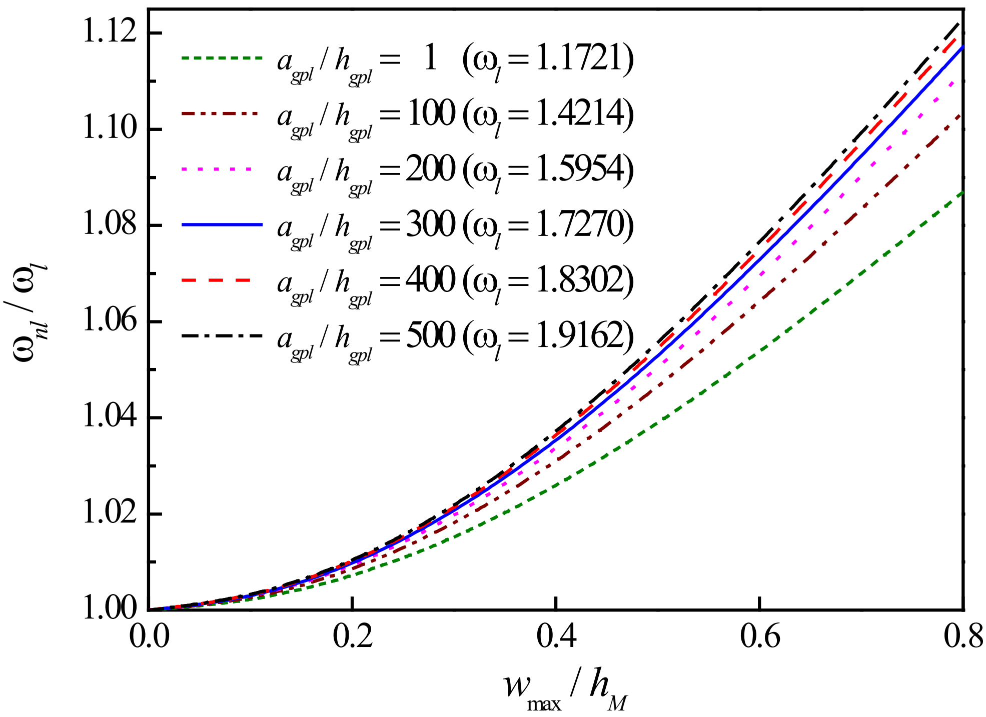

1.12
1.10
1.08
1.06
1.04
1.02
1.00
0.0
0.2
0.4
0.6
0.8
ω_{nl} / ω_l
$w_{\max} / h_M$
$a_{gpl} / h_{gpl} = 1 \ (\omega_l = 1.1721)$
$a_{gpl} / h_{gpl} = 100 \ (\omega_l = 1.4214)$
$a_{gpl} / h_{gpl} = 200 \ (\omega_l = 1.5954)$
$a_{gpl} / h_{gpl} = 300 \ (\omega_l = 1.7270)$
$a_{gpl} / h_{gpl} = 400 \ (\omega_l = 1.8302)$
$a_{gpl} / h_{gpl} = 500 \ (\omega_l = 1.9162)$

Figure 16